

# Forward and backward in time dispersion of fluid and inertial particles in isotropic turbulence

Andrew D. Bragg, Peter J. Ireland and Lance R. Collins

Sibley School of Mechanical & Aerospace Engineering, Cornell University, Ithaca, NY 14853

March 24, 2014

## Abstract

In this paper we investigate both theoretically and numerically the forward and backward in time mean square separation of fluid and inertial particle pairs in isotropic turbulence. Fluid particles are known to separate faster backward in time than forward in time, and we find that inertial particles do the same. However, we find that the time asymmetry in their dispersion is in general much greater than for fluid particles. Whereas the time-irreversibility of fluid particle pair dispersion can be understood in terms of a directional bias arising from the dissipative dynamics of turbulence, inertial particles experience an additional source of irreversibility arising from a symmetry breaking path history effect of their inertia. For each given initial (final, in the backward in time case) separation  $\mathbf{r}^0$  there is an optimum value of the particle momentum response time,  $\tau_p$ , for which the particles are most strongly affected by the time reversal since those particles are optimally affected by both sources of irreversibility. We derive analytical expressions for the backward in time mean square separation of inertial particles and compare the predictions with numerical data obtained from a  $Re_\lambda \approx 580$  DNS of particle laden isotropic turbulent flow. For times  $\leq \max[\tau_p, \tau_{r^0}]$  (where  $\tau_{r^0}$  is the timescale of the fluid velocity differences at separation  $\mathbf{r}^0 = |\mathbf{r}^0|$ ), we find excellent agreement between the theoretical predictions and the DNS. The theory for times  $> \max[\tau_p, \tau_{r^0}]$  is in good agreement with the DNS provided that the pair separation at these times exceeds a few multiples of the Kolmogorov spatial scale  $\eta$ .

## 1 Introduction

The relative motion of fluid particles in turbulent flows has been a subject of intense investigation since the pioneering studies of Taylor [1] and Richardson [2]. The subject has attracted great interest both because of the theoretical challenges it poses and also because of its importance in a broad range of environmental and industrial applications.

The traditional scenario involves forward in time (FIT) dispersion, that is, the variation in time of pairs of fluid particles which have a given initial separation. Much of the work has focused on the mean square separation  $\langle |\mathbf{r}^f(t)|^2 \rangle_{\mathbf{r}'}$ , where  $\mathbf{r}^f(t)$  is the fluid particle relative separation vector and  $\langle \cdot \rangle_{\mathbf{r}'}$  denotes an ensemble average conditioned on  $\mathbf{r}^f(t') = \mathbf{r}'$  with  $t' \leq t$ . Several theoretical predictions for  $\langle |\mathbf{r}^f(t)|^2 \rangle_{\mathbf{r}'}$  for varying  $\mathbf{r}'$  and  $t$  have been developed which we shall discuss in §3.1. For extensive reviews of this topic see [3, 4].

In [5] the backward in time (BIT) dispersion of fluid particles was investigated and compared with the FIT dispersion. BIT dispersion concerns the behavior of particle pairs which *arrive* at

a given location at a given time and which were dispersed at times in the past (i.e. a given end condition, in contrast to FIT dispersion where it is a given initial condition). The BIT mean square separation may be denoted as  $\langle |\mathbf{r}^f(t')|^2 \rangle_{\mathbf{r}}$ , where  $\mathbf{r}^f(t')$  is the fluid particle relative separation vector and  $\langle \cdot \rangle_{\mathbf{r}}$  denotes an ensemble average conditioned on  $\mathbf{r}^f(t) = \mathbf{r}$  with  $t' \leq t$ . Sawford *et al.* [5] note that it is BIT dispersion, not FIT dispersion that is connected to mixing processes, and therefore understanding BIT dispersion is of great importance to developing the understanding and modeling of mixing processes.

A point worth emphasizing to avoid confusion is that in BIT dispersion, the underlying dynamical system is not actually evolving backward in time. Rather it is evolving forward in time; the dispersion is BIT only in the sense that one is considering the positions of particles at earlier times  $t'$ , given their position at time  $t$ .

Compared to the relative dispersion of fluid particles, that of inertial particles has only recently begun to be investigated. The most comprehensive study to date is that of Bec *et al.* [6] where they used DNS data to investigate the FIT dispersion of inertial particles and also developed mean-field theoretical descriptions of the dispersion process. Theoretical work on the FIT dispersion of inertial particles has also been done for limiting cases such as  $St \gg 1$  [7] and time uncorrelated flows [8]. The present study is inspired by [6] and takes the study to a next step by considering the BIT dispersion of inertial particles, comparing this to the FIT dispersion and seeking to provide both theoretical predictions and physical explanations for the time-irreversability of the inertial particle pair dispersion.

A motivation for this work is also that it provides insight into how the theory in [9] might be improved since the authors identify the importance of a correct understanding of the BIT dispersion of inertial particles for their relative velocity theory and yet note that such a study has not yet been undertaken. The importance of developing a BIT dispersion theory in order to improve the relative velocity theory in [9] was highlighted in [10].

## 2 Governing equations and general solutions

In this section we construct the exact, but unclosed, expressions for the FIT and BIT mean square separation of the inertial particles which will be used in subsequent sections as the basis from which to derive closed, analytical expressions for these quantities.

We consider the relative dispersion of monodisperse inertial particles subject to Stokes drag forcing in isotropic turbulence. The equation governing their relative motion is then obtained from the simplified form of the Maxey-Riley equation [11]

$$\frac{d^2}{dt^2} \mathbf{r}^p(t) = \frac{d}{dt} \mathbf{w}^p(t) = \frac{1}{\tau_p} \left( \Delta \mathbf{u}^p(t) - \mathbf{w}^p(t) \right), \quad (1)$$

where  $\mathbf{r}^p(t)$ ,  $\mathbf{w}^p(t)$  are the inertial particle pair relative position and relative velocity vectors,  $\tau_p$  is the momentum response time of the particles and  $\Delta \mathbf{u}^p(t) = \Delta \mathbf{u}(\mathbf{r}^p(t), t)$  is the difference between the fluid velocity field evaluated at the positions of the two particles. Here and throughout the superscript ‘ $p$ ’ denotes that the variable is defined along inertial particle trajectories, and in the limit of zero inertia we will sometimes replace this superscript with ‘ $f$ ’ to denote that in this limit

we are considering fluid particles. The formal solution to (1) may be written as

$$\mathbf{r}^p(t) = \mathbf{r}^p(t') + G(t-t')\mathbf{w}^p(t') + \tau_p^{-1} \int_{t'}^t G(t-s)\Delta\mathbf{u}^p(s)ds, \quad t' \leq t, \quad (2)$$

$$\mathbf{w}^p(t) = \dot{G}(t-t')\mathbf{w}^p(t') + \tau_p^{-1} \int_{t'}^t \dot{G}(t-s)\Delta\mathbf{u}^p(s)ds, \quad t' \leq t, \quad (3)$$

where  $G$  is the Green function for the equation of motion for  $\mathbf{r}^p(t)$  and

$$G(t-t') = \tau_p \left(1 - \exp[-\tau_p^{-1}(t-t')]\right), \quad (4)$$

$$\dot{G}(t-t') = \exp[-\tau_p^{-1}(t-t')]. \quad (5)$$

The FIT dispersion PDF is defined as

$$\varrho^F(\mathbf{r}, t | \mathbf{r}', t') = \left\langle \delta(\mathbf{r}^p(t) - \mathbf{r}) \right\rangle_{\mathbf{r}'}, \quad (6)$$

and for BIT dispersion

$$\varrho^B(\mathbf{r}', t' | \mathbf{r}, t) = \left\langle \delta(\mathbf{r}^p(t') - \mathbf{r}') \right\rangle_{\mathbf{r}}, \quad (7)$$

and in each case  $t' \leq t$ . The notation  $\langle \cdot \rangle_{\mathbf{r}'}$  and  $\langle \cdot \rangle_{\mathbf{r}}$  in (6) and (7) denote conditional ensemble averaging; conditioned on  $\mathbf{r}^p(t') = \mathbf{r}'$  in the FIT case ('initial time conditioning') and  $\mathbf{r}^p(t) = \mathbf{r}$  in the BIT case ('end time conditioning'). In this paper we are interested in the mean square separation behavior rather than the full dispersion PDF. From (6) and (7) we may define the FIT and BIT mean square separation

$$\left\langle |\mathbf{r}^p(t)|^2 \right\rangle_{\mathbf{r}'} = \int_{\mathbf{r}} \mathbf{r} \cdot \mathbf{r} \varrho^F(\mathbf{r}, t | \mathbf{r}', t') d\mathbf{r}, \quad (8)$$

$$\left\langle |\mathbf{r}^p(t')|^2 \right\rangle_{\mathbf{r}} = \int_{\mathbf{r}'} \mathbf{r}' \cdot \mathbf{r}' \varrho^B(\mathbf{r}', t' | \mathbf{r}, t) d\mathbf{r}'. \quad (9)$$

We may construct an exact expression for (8) using (2)

$$\begin{aligned} \left\langle |\mathbf{r}^p(t)|^2 \right\rangle_{\mathbf{r}'} &= \mathbf{r}' \cdot \mathbf{r}' + 2G(t-t')\mathbf{r}' \cdot \left\langle \mathbf{w}^p(t') \right\rangle_{\mathbf{r}'} + 2\tau_p^{-1}\mathbf{r}' \cdot \int_{t'}^t G(t-s) \left\langle \Delta\mathbf{u}^p(s) \right\rangle_{\mathbf{r}'} ds \\ &\quad + G^2(t-t') \left\langle \mathbf{w}^p(t') \cdot \mathbf{w}^p(t') \right\rangle_{\mathbf{r}'} + 2\tau_p^{-1}G(t-t') \int_{t'}^t G(t-s) \left\langle \mathbf{w}^p(t') \cdot \Delta\mathbf{u}^p(s) \right\rangle_{\mathbf{r}'} ds \\ &\quad + \tau_p^{-2} \int_{t'}^t \int_{t'}^t G(t-s)G(t-s') \left\langle \Delta\mathbf{u}^p(s) \cdot \Delta\mathbf{u}^p(s') \right\rangle_{\mathbf{r}'} ds' ds, \end{aligned} \quad (10)$$

and rearranging (2) for  $\mathbf{r}^p(t')$  we may construct the expression for (9)

$$\begin{aligned}
\left\langle |\mathbf{r}^p(t')|^2 \right\rangle_{\mathbf{r}} &= \mathbf{r} \cdot \mathbf{r} - 2G(t-t') \mathbf{r} \cdot \left\langle \mathbf{w}^p(t') \right\rangle_{\mathbf{r}} - 2\tau_p^{-1} \mathbf{r} \cdot \int_{t'}^t G(t-s) \left\langle \Delta \mathbf{u}^p(s) \right\rangle_{\mathbf{r}} ds \\
&+ G^2(t-t') \left\langle \mathbf{w}^p(t') \cdot \mathbf{w}^p(t') \right\rangle_{\mathbf{r}} + 2\tau_p^{-1} G(t-t') \int_{t'}^t G(t-s) \left\langle \mathbf{w}^p(t') \cdot \Delta \mathbf{u}^p(s) \right\rangle_{\mathbf{r}} ds \\
&+ \tau_p^{-2} \int_{t'}^t \int_{t'}^t G(t-s) G(t-s') \left\langle \Delta \mathbf{u}^p(s) \cdot \Delta \mathbf{u}^p(s') \right\rangle_{\mathbf{r}} ds' ds.
\end{aligned} \tag{11}$$

Since we are interested in statistically stationary systems we may set the ‘conditioning time’ to zero and consider the dispersion behavior as a function of time separation. In the FIT case this amounts to setting  $t' = 0$  and in the BIT case setting  $t = 0$ . Further, since  $t' \leq t$  we may re-write (10) and (11) as

$$\begin{aligned}
\left\langle |\mathbf{r}^p(\mathcal{T})|^2 \right\rangle_{\mathbf{r}^0} &= \mathbf{r}^0 \cdot \mathbf{r}^0 + 2G(\mathcal{T}) \mathbf{r}^0 \cdot \left\langle \mathbf{w}^p(0) \right\rangle_{\mathbf{r}^0} + 2\tau_p^{-1} \mathbf{r}^0 \cdot \int_0^{\mathcal{T}} G(\mathcal{T}-s) \left\langle \Delta \mathbf{u}^p(s) \right\rangle_{\mathbf{r}^0} ds \\
&+ G^2(\mathcal{T}) \left\langle \mathbf{w}^p(0) \cdot \mathbf{w}^p(0) \right\rangle_{\mathbf{r}^0} + 2\tau_p^{-1} G(\mathcal{T}) \int_0^{\mathcal{T}} G(\mathcal{T}-s) \left\langle \mathbf{w}^p(0) \cdot \Delta \mathbf{u}^p(s) \right\rangle_{\mathbf{r}^0} ds \tag{12} \\
&+ \tau_p^{-2} \int_0^{\mathcal{T}} \int_0^{\mathcal{T}} G(\mathcal{T}-s) G(\mathcal{T}-s') \left\langle \Delta \mathbf{u}^p(s) \cdot \Delta \mathbf{u}^p(s') \right\rangle_{\mathbf{r}^0} ds' ds,
\end{aligned}$$

where  $\mathcal{T} = t - t'$  with  $t' = 0$ ,  $t' \leq t$  so that  $\mathcal{T} \geq 0$  and

$$\begin{aligned}
\left\langle |\mathbf{r}^p(-\mathcal{T})|^2 \right\rangle_{\mathbf{r}^0} &= \mathbf{r}^0 \cdot \mathbf{r}^0 - 2G(\mathcal{T}) \mathbf{r}^0 \cdot \left\langle \mathbf{w}^p(-\mathcal{T}) \right\rangle_{\mathbf{r}^0} - 2\tau_p^{-1} \mathbf{r}^0 \cdot \int_{-\mathcal{T}}^0 G(-s) \left\langle \Delta \mathbf{u}^p(s) \right\rangle_{\mathbf{r}^0} ds \\
&+ G^2(\mathcal{T}) \left\langle \mathbf{w}^p(-\mathcal{T}) \cdot \mathbf{w}^p(-\mathcal{T}) \right\rangle_{\mathbf{r}^0} + 2\tau_p^{-1} G(\mathcal{T}) \int_{-\mathcal{T}}^0 G(-s) \left\langle \mathbf{w}^p(-\mathcal{T}) \cdot \Delta \mathbf{u}^p(s) \right\rangle_{\mathbf{r}^0} ds \\
&+ \tau_p^{-2} \int_{-\mathcal{T}}^0 \int_{-\mathcal{T}}^0 G(-s) G(-s') \left\langle \Delta \mathbf{u}^p(s) \cdot \Delta \mathbf{u}^p(s') \right\rangle_{\mathbf{r}^0} ds' ds,
\end{aligned} \tag{13}$$

where again  $\mathcal{T} = t - t'$  but now with  $t = 0$ ,  $t' \leq t$  so that  $\mathcal{T} \geq 0$  and  $t' = -\mathcal{T}$ , and  $\langle \cdot \rangle_{\mathbf{r}^0}$  denotes an ensemble average conditioned on  $\mathbf{r}^p(\mathcal{T} = 0) = \mathbf{r}^0$ . In going from (11) to (13)

$$G(t-t') = \tau_p \left( 1 - \exp[-\tau_p^{-1}(t-t')] \right) = \tau_p \left( 1 - \exp[-\tau_p^{-1}\mathcal{T}] \right) = G(\mathcal{T}),$$

and

$$G(t-s) = \tau_p \left( 1 - \exp[-\tau_p^{-1}(t-s)] \right) = \tau_p \left( 1 - \exp[\tau_p^{-1}s] \right) = G(-s).$$

We may develop theoretical descriptions for the FIT and BIT dispersion of inertial particles by applying closure approximations to (12) and (13) to construct closed analytical solutions. The mean square separation of fluid particles governed by the evolution equation  $\dot{\mathbf{r}}^f(t) = \Delta \mathbf{u}(\mathbf{r}^f(t), t)$  can also be constructed using (12) and (13) by taking the limit  $\tau_p \rightarrow 0$ .

Note that an alternative way to construct the BIT results would be to construct them from the solutions to the time reversed form of the equations of motion. We have not chosen to construct the BIT results via this method because we believe it hinders the physical understanding: In DNS, for example, we obtain the BIT statistics by recording the trajectories of particles evolved using the standard forward in time equations of motion, and then subsequently evaluate the BIT statistics based on the particle trajectory histories (i.e., in DNS the BIT trajectories are not obtained by solving the time reversed form of the dynamical equations). Therefore we have constructed (13) in a manner consistent with how the same statistics are obtained in DNS (and experiment), which aids the physical interpretation and explanation of the results.

We will first consider the case of fluid particle dispersion which will be helpful before considering the more complex scenario of inertial particle dispersion.

### 3 Fluid particle dispersion

#### 3.1 Theory

The FIT and BIT mean square dispersion of fluid particles is given by (12) and (13) when  $\tau_p = 0$  (we replace the superscript ‘ $p$ ’ with ‘ $f$ ’ in (12) and (13) to denote that we are now considering fluid particles). Following Batchelor [12], for small  $\mathcal{T}$  we may make the approximation  $\Delta \mathbf{u}^f(\dots) \approx \Delta \mathbf{u}^f(0)$ . Introducing this approximation into (12) and (13) we obtain for  $\tau_p = 0$

$$\left\langle |\mathbf{r}^f(\mathcal{T})|^2 \right\rangle_{\mathbf{r}^0} \approx \left\langle |\mathbf{r}^f(-\mathcal{T})|^2 \right\rangle_{\mathbf{r}^0} \approx |\mathbf{r}^0|^2 + \mathcal{T}^2 \left\langle |\Delta \mathbf{u}^f(0)|^2 \right\rangle_{\mathbf{r}^0}. \quad (14)$$

This ballistic behavior is expected to be valid up to times of the order of the correlation timescale of  $\Delta \mathbf{u}$  for separations of size  $\mathbf{r}^0$ , known as the Batchelor timescale  $\tau_{r^0}$ . For initial separations in the dissipation regime we take  $\tau_{r^0} = \tau_\eta$  and in the inertial range  $\tau_{r^0} = (|\mathbf{r}^0|^2 / \langle \epsilon \rangle)^{1/3}$ . Notice that in the ballistic regime the fluid particle dispersion is time reversible because  $\Delta \mathbf{u}^f(\dots) \approx \Delta \mathbf{u}^f(0)$  ignores the dynamical evolution of  $\Delta \mathbf{u}^f$  along the pair trajectories.

In [13] the authors consider the importance of correctly including the terms involving  $\mathbf{r}^0$  in the description of the mean square separation (this is also discussed in [4]). Specifically they consider the difference between (14) and

$$\left\langle |\mathbf{r}^f(\mathcal{T}) - \mathbf{r}^0|^2 \right\rangle_{\mathbf{r}^0} \approx \mathcal{T}^2 \left\langle |\Delta \mathbf{u}^f(0)|^2 \right\rangle_{\mathbf{r}^0}. \quad (15)$$

We may write

$$\left\langle |\mathbf{r}^f(\mathcal{T}) - \mathbf{r}^0|^2 \right\rangle_{\mathbf{r}^0} = \left\langle |\mathbf{r}^f(\mathcal{T})|^2 \right\rangle_{\mathbf{r}^0} - 2\mathbf{r}^0 \cdot \left\langle \mathbf{r}^f(\mathcal{T}) \right\rangle_{\mathbf{r}^0} + |\mathbf{r}^0|^2, \quad (16)$$

showing that a difference between (14) and (15) arises when  $\langle \mathbf{r}^f(\mathcal{T}) \rangle_{\mathbf{r}^0} \neq \mathbf{r}^0$ . The solution for  $\langle \mathbf{r}^f(\mathcal{T}) \rangle_{\mathbf{r}^0}$  is given by

$$\left\langle \mathbf{r}^f(\mathcal{T}) \right\rangle_{\mathbf{r}^0} = \mathbf{r}^0 + \int_0^{\mathcal{T}} \left\langle \Delta \mathbf{u}^f(s) \right\rangle_{\mathbf{r}^0} ds, \quad (17)$$

giving

$$\left\langle |\mathbf{r}^f(\mathcal{T}) - \mathbf{r}^0|^2 \right\rangle_{\mathbf{r}^0} = \left\langle |\mathbf{r}^f(\mathcal{T})|^2 \right\rangle_{\mathbf{r}^0} - |\mathbf{r}^0|^2 - 2\mathbf{r}^0 \cdot \int_0^{\mathcal{T}} \left\langle \Delta \mathbf{u}^f(s) \right\rangle_{\mathbf{r}^0} ds, \quad (18)$$

whose terms may be identified in (12) in the limit  $\tau_p \rightarrow 0$ . In [13] the authors find that if they plot their experimental data for

$$\left\langle |\mathbf{r}^f(\mathcal{T}) - \mathbf{r}^0|^2 \right\rangle_{\mathbf{r}^0} / \mathcal{T}^2 \left\langle |\Delta \mathbf{u}^f(0)|^2 \right\rangle_{\mathbf{r}^0},$$

they find a good collapse, verifying the validity of the ballistic prediction. However when they plot

$$\left( \left\langle |\mathbf{r}^f(\mathcal{T})|^2 \right\rangle_{\mathbf{r}^0} - |\mathbf{r}^0|^2 \right) / \mathcal{T}^2 \left\langle |\Delta \mathbf{u}^f(0)|^2 \right\rangle_{\mathbf{r}^0},$$

they do not find a good collapse of data indicating that the term of difference between the two is important. From (18) we see that the difference between these two expressions depends upon the integral of  $\langle \Delta \mathbf{u}^f(s) \rangle_{\mathbf{r}^0}$ . The ballistic results in (14) and (15) are derived under the approximation  $\Delta \mathbf{u}^f(\cdot \cdot) \approx \Delta \mathbf{u}^f(0)$  which gives  $\langle \Delta \mathbf{u}^f(0) \rangle_{\mathbf{r}^0}$ . For fully mixed fluid particles in isotropic turbulence this term is zero, and therefore under the ballistic approximation

$$\left\langle |\mathbf{r}^f(\mathcal{T}) - \mathbf{r}^0|^2 \right\rangle_{\mathbf{r}^0} = \left\langle |\mathbf{r}^f(\mathcal{T})|^2 \right\rangle_{\mathbf{r}^0} - |\mathbf{r}^0|^2. \quad (19)$$

Consequently the results in [13] for the ballistic case are surprising since in this regime there should be no difference between (14) and (15). In §3.2 we will consider this using DNS data.

In general, however,  $\langle \Delta \mathbf{u}^f(s) \rangle_{\mathbf{r}^0} \neq \mathbf{0}$  even for isotropic turbulence. The reason is the conditional nature of the average; particle pairs which were at  $\mathbf{r}^0$  at  $\mathcal{T} = 0$  and are on average separating will be experiencing positive velocity differences on average, i.e.  $\langle \Delta \mathbf{u}^f(s) \rangle_{\mathbf{r}^0} \geq \mathbf{0}$ . Nevertheless, we expect that the effect of this on the prediction of  $\langle |\mathbf{r}^f(\mathcal{T})|^2 \rangle_{\mathbf{r}^0}$  will be small compared to the higher order moment terms in its evolution equation. Similar arguments also describe the BIT case, only in that case since fluid particles are on average approaching each other towards  $\mathbf{r}^0$  then  $\langle \Delta \mathbf{u}^f(s) \rangle_{\mathbf{r}^0} \leq \mathbf{0}$ .

The ballistic approximation described above should be applicable for  $\mathcal{T} \lesssim \tau_{r^0}$  and all  $\mathbf{r}^0$ . However in the dissipation regime where  $\Delta \mathbf{u}$  is linear in  $\mathbf{r}$  we may improve upon the approximation  $\Delta \mathbf{u}^f(\cdot \cdot) \approx \Delta \mathbf{u}^f(0)$ . In the dissipation regime  $\Delta \mathbf{u} = \mathbf{\Gamma} \cdot \mathbf{r}$  where  $\mathbf{\Gamma}$  is the fluid velocity gradient tensor. Introducing this into (12) for  $\tau_p = 0$  we have

$$\begin{aligned} \left\langle |\mathbf{r}^f(\mathcal{T})|^2 \right\rangle_{\mathbf{r}^0} = & |\mathbf{r}^0|^2 + 2\mathbf{r}^0 \cdot \int_0^{\mathcal{T}} \left\langle \mathbf{\Gamma}^f(s) \cdot \mathbf{r}^f(s) \right\rangle_{\mathbf{r}^0} ds \\ & + \int_0^{\mathcal{T}} \int_0^{\mathcal{T}} \left\langle \left( \mathbf{\Gamma}^f(s) \cdot \mathbf{r}^f(s) \right) \cdot \left( \mathbf{\Gamma}^f(s') \cdot \mathbf{r}^f(s') \right) \right\rangle_{\mathbf{r}^0} ds' ds. \end{aligned} \quad (20)$$

Next we make the essentially local approximations  $\langle \mathbf{\Gamma}^f(s) \rangle_{\mathbf{r}^0} \approx \langle \mathbf{\Gamma}^f(0) \rangle_{\mathbf{r}^0} = \mathbf{0}$  and  $\mathbf{r}^f(s) \approx \mathbf{r}^f(s') \approx \mathbf{r}^f(0) = \mathbf{r}^0$  and also

$$\left\langle \mathbf{\Gamma}^f(s) \cdot \mathbf{\Gamma}^f(s') \right\rangle_{\mathbf{r}^0} \approx \left\langle \mathbf{S} \cdot \mathbf{S} \right\rangle \exp \left[ -\frac{s-s'}{\tau_S} \right] + \left\langle \mathbf{R} \cdot \mathbf{R} \right\rangle \exp \left[ -\frac{s-s'}{\tau_R} \right], \quad (21)$$

where  $\mathcal{S}$  and  $\mathcal{R}$  are the strain-rate and rotation-rate tensors and  $\tau_{\mathcal{S}}$  and  $\tau_{\mathcal{R}}$  are their associated Lagrangian timescales. The above approximations improve upon the ballistic approximation in the dissipation regime in that the ballistic approximation uses  $\Delta \mathbf{u}(\mathbf{r}^f(s), s) \approx \mathbf{\Gamma}^f(0) \cdot \mathbf{r}^f(0)$  whereas we now have  $\Delta \mathbf{u}(\mathbf{r}^f(s), s) \approx \mathbf{\Gamma}^f(s) \cdot \mathbf{r}^f(0)$ . Introducing these approximations into (20) and solving the integrals we obtain for isotropic turbulence

$$\begin{aligned} \left\langle |\mathbf{r}^f(\mathcal{T})|^2 \right\rangle_{\mathbf{r}^0} = & |\mathbf{r}^0|^2 + \frac{\langle \epsilon \rangle}{6\nu} |\mathbf{r}^0|^2 \tau_{\mathcal{S}}^2 \left( \exp[\tau_{\mathcal{S}}^{-1} \mathcal{T}] + \exp[-\tau_{\mathcal{S}}^{-1} \mathcal{T}] - 2 \right) \\ & + \frac{\langle \epsilon \rangle}{6\nu} |\mathbf{r}^0|^2 \tau_{\mathcal{R}}^2 \left( \exp[\tau_{\mathcal{R}}^{-1} \mathcal{T}] + \exp[-\tau_{\mathcal{R}}^{-1} \mathcal{T}] - 2 \right), \end{aligned} \quad (22)$$

where  $\langle \epsilon \rangle$  is the mean turbulent kinetic energy dissipation rate and  $\nu$  is the fluid kinematic viscosity. It may seem surprising that rotation is present in the above result since the well known differential law

$$\frac{d}{d\mathcal{T}} \left\langle |\mathbf{r}^f(\mathcal{T})|^2 \right\rangle_{\mathbf{r}^0} = 2 \left\langle (\mathbf{r}^f(\mathcal{T}) \mathbf{r}^f(\mathcal{T})) : \mathcal{S}^f(\mathcal{T}) \right\rangle_{\mathbf{r}^0}, \quad (23)$$

seems to imply that only strain contributes to the mean square separation growth. However the expression in (23) does contain the effect of rotation implicitly since  $\mathbf{r}^f(\mathcal{T})$  depends upon the history of both strain and rotation along the fluid particle pair trajectory, so that rotation contributes to the mean square separation of the particles through its effect upon the alignment between  $\mathbf{r}^f(\mathcal{T})$  and  $\mathcal{S}^f(\mathcal{T})$ .

The result in (22) differs from the result ascribed to Batchelor (e.g. [14]), namely

$$\left\langle |\mathbf{r}^f(\mathcal{T})|^2 \right\rangle_{\mathbf{r}^0} = |\mathbf{r}^0|^2 \exp[2B\tau_{\eta}^{-1} \mathcal{T}], \quad (24)$$

where various values for  $B$  have been given (see [14]). This result seems to be based on Batchelor's finding in [15] Eq. (2.8) that fluid particle pairs in the dissipation range separate exponentially. However in [15] it is stated that Eq. (2.8) is the result for large  $\mathcal{T}$ , which when squared and averaged gives (24). Consequently the Batchelor exponential law is not strictly valid for small  $\mathcal{T}$ . The result in (22) is a more general result valid also at small  $\mathcal{T}$ , and which does in fact grow exponentially for large  $\mathcal{T}$  in keeping with Batchelor's long time prediction. Furthermore, note that for small  $\mathcal{T}$  we may expand the exponential terms in (22) to obtain

$$\left\langle |\mathbf{r}^f(\mathcal{T})|^2 \right\rangle_{\mathbf{r}^0} = |\mathbf{r}^0|^2 + \frac{\langle \epsilon \rangle}{3\nu} |\mathbf{r}^0|^2 \mathcal{T}^2 + \mathcal{O}(\mathcal{T}^3), \quad (25)$$

which is nothing other than (14) for  $\mathbf{r}^0$  in the dissipation regime. Therefore the result in (22) describes both the initial ballistic separation of the fluid particles and also the subsequent exponential growth. The result in (22) should be valid provided that both  $|\mathbf{r}^0|$  and  $\sqrt{\langle |\mathbf{r}^f(\mathcal{T})|^2 \rangle_{\mathbf{r}^0}}$  lie in the regime for which  $\Delta \mathbf{u}$  is linear in  $\mathbf{r}$ , i.e. the dissipation regime. Though formally the dissipation regime is defined for  $|\mathbf{r}| \ll \eta$ , high  $Re_{\lambda}$  DNS data suggests that  $\Delta \mathbf{u}$  is approximately linear in  $\mathbf{r}$  up to  $|\mathbf{r}| \sim 10\eta$  [16].

Under the approximations invoked in the derivation of (22) the equivalent BIT result is identical because the timescales of  $\mathcal{S}$  and  $\mathcal{R}$  are the same FIT and BIT (at least for isotropic turbulence). However since BIT dispersion is in general faster than FIT dispersion the approximation  $\mathbf{r}^f(s) \approx \mathbf{r}^f(s') \approx \mathbf{r}^f(0) = \mathbf{r}^0$  is likely to break down at smaller time separations than in the FIT case. We will consider this when we compare (22) with DNS data in §3.2.

If  $\mathbf{r}^0$  lies in the inertial range of scales (i.e.  $\eta \ll |\mathbf{r}^0| \ll L$  where  $\eta$  and  $L$  are the Kolmogorov and integral lengthscales) then K41 theory may be used to describe the behavior of the fluid velocity differences in (12) and (13) for  $\tau_p = 0$  and obtain the result for large  $\mathcal{T}$  in the inertial range

$$\left\langle |\mathbf{r}^f(\mathcal{T})|^2 \right\rangle_{\mathbf{r}^0} = |\mathbf{r}^0|^2 + \mathfrak{g}^F \langle \epsilon \rangle \mathcal{T}^3, \quad (26)$$

$$\left\langle |\mathbf{r}^f(-\mathcal{T})|^2 \right\rangle_{\mathbf{r}^0} = |\mathbf{r}^0|^2 + \mathfrak{g}^B \langle \epsilon \rangle \mathcal{T}^3, \quad (27)$$

where  $\mathfrak{g}^F$  and  $\mathfrak{g}^B$  are the FIT and BIT Richardson's constants, estimated from experimental data to be  $\mathfrak{g}^F \approx 0.55$  and  $\mathfrak{g}^B \approx 1.15$  [17]. The result in (26) is from Batchelor's work [12] and (27), the BIT equivalent of (26), was proposed by Sawford *et al.* [5]. It is also conventional to refer to the  $\mathcal{T}^3$  scaling law as the Richardson-Obukhov (RO) law.

If  $\mathbf{r}^0 > L$  then the dispersion (following the initial ballistic separation) is diffusive and time reversible. This is because at these separations the two particles experience no correlation between their motion, and also because the large scale motions of the turbulence which drive the relative dispersion for  $\mathbf{r}^0 > L$  are approximately time reversible.

Different explanations have been given for why FIT and BIT fluid particle dispersion at sub-integral scales differ. In [5] the behavior of the odd-moments of the velocity increments in turbulence under time reversal was used to provide an explanation for the difference between forward and backward dispersion. In [17] the authors appealed to the behavior of the eigenvalues of the turbulence strain tensor under time reversal to explain the difference; the largest eigenvalue for the BIT turbulent strain tensor is larger than the largest eigenvalue for the FIT strain tensor, thus explaining, at least partially, why BIT dispersion is faster than FIT dispersion. They also argued that since the course grained strain tensor exhibits similar dynamics to the viscous counterpart, their argument applies for dispersion in the inertial range of the turbulence.

A simple qualitative explanation is to recognize the role of the energy transfer from the large to small scales in turbulence. In BIT dispersion where pairs are on average converging to smaller separations, the convergence is aided by the energy transfer, whereas in FIT dispersion where pairs are separating the energy transfer acts against their separation and thus BIT dispersion is faster than FIT dispersion. This argument also suggests that in 2D turbulence where there is an inverse energy cascade, FIT dispersion should be faster than BIT dispersion, something which appears to have been shown in [18].

What each of these explanations share in common is that the time-irreversibility of fluid particle dispersion in turbulence is explained as arising, fundamentally, because of the intrinsic time directionality in turbulence dynamics, a consequence of its dissipative nature. We note however that although this is the physical origin of the irreversibility in Navier-Stokes turbulence, any model which generates asymmetric probability density functions for  $\Delta \mathbf{u}(\mathbf{r}, t)$  would give rise to irreversible fluid particle pair dispersion.

### 3.2 DNS results

We now consider results from a DNS of statistically stationary, homogeneous, isotropic turbulence at  $Re_\lambda \approx 580$  against which we will test the theoretical results discussed in §3.1. Details of the DNS can be found in appendix A.

We begin by showing the effects of time reversal on the mean square separation in Figure 1.



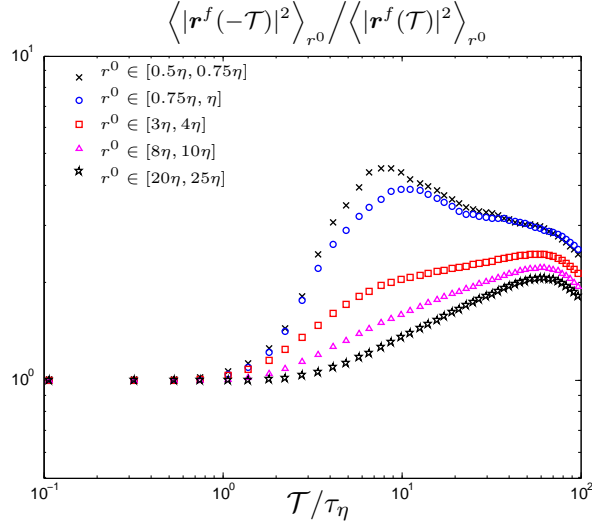


Figure 1: DNS data for the ratio of the BIT to FIT mean square separation of fluid particles as a function of  $\mathcal{T}$  for varying  $r^0$ .

The results in Fig. 1 clearly show the effects of time reversal, with BIT greater than FIT dispersion. The results also show that the peak in the ratio increases with decreasing  $r^0$ . The time it takes for the ratio to begin to increase from unity increases with increasing  $r^0$ . This is because the initial ballistic motion, in which the separation is time reversible, is supposed to persist for  $\mathcal{T} \lesssim \tau_{r^0}$  and  $\tau_{r^0}$  increases with increasing  $r^0$ . For  $r^0 > L$ , where  $L$  is the integral length scale of the flow ( $L/\eta \approx 800$  for this DNS), the ratio would be unity since the motion of the large scales is approximately time reversible.

In Fig. 2 we plot the DNS data for  $(\langle |\mathbf{r}^f(\mathcal{T})|^2 \rangle_{r^0} - |\mathbf{r}^0|^2)/\tau_\eta^2 \langle |\Delta \mathbf{u}^f(0)| \rangle_{r^0}$  and  $(\langle |\mathbf{r}^f(-\mathcal{T})|^2 \rangle_{r^0} - |\mathbf{r}^0|^2)/\tau_\eta^2 \langle |\Delta \mathbf{u}^f(0)| \rangle_{r^0}$  (here and throughout, we use the DNS data for  $\langle |\Delta \mathbf{u}^f(0)| \rangle_{r^0}$ ). The data shows a good collapse for small  $\mathcal{T}$  for both the FIT and BIT cases, demonstrating the accuracy of (14) for small  $\mathcal{T}$ , and also that the duration of the ballistic regime increases with increasing  $r^0$ . In §3.1 we argued that under the approximation for which the ballistic behavior is predicted

$$\langle |\mathbf{r}^f(\mathcal{T}) - \mathbf{r}^0|^2 \rangle_{r^0} = \langle |\mathbf{r}^f(\mathcal{T})|^2 \rangle_{r^0} - |\mathbf{r}^0|^2,$$

and the results in Fig. 2 by implication confirm the validity of this approximation. In [13] the authors argue and show results (see Fig. 6 in their paper) which seem to indicate that

$$\langle |\mathbf{r}^f(\mathcal{T}) - \mathbf{r}^0|^2 \rangle_{r^0} \approx \langle |\mathbf{r}^f(\mathcal{T})|^2 \rangle_{r^0} - |\mathbf{r}^0|^2,$$

even in the ballistic limit. However we question the data presented in Fig. 6 of [13] since it implies

$$\left( \langle |\mathbf{r}^f(\mathcal{T})|^2 \rangle_{r^0} - |\mathbf{r}^0|^2 \right) / \tau_\eta^2 \langle |\Delta \mathbf{u}^f(0)| \rangle_{r^0} \rightarrow \text{finite value as } \mathcal{T} \rightarrow 0,$$

which cannot be correct (by definition  $\langle |\mathbf{r}^f(\mathcal{T})|^2 \rangle_{r^0} - |\mathbf{r}^0|^2 \rightarrow 0$  as  $\mathcal{T} \rightarrow 0$ ). One explanation for this may be errors introduced by the relatively large size of their bins, having widths  $\approx 43\eta$ .

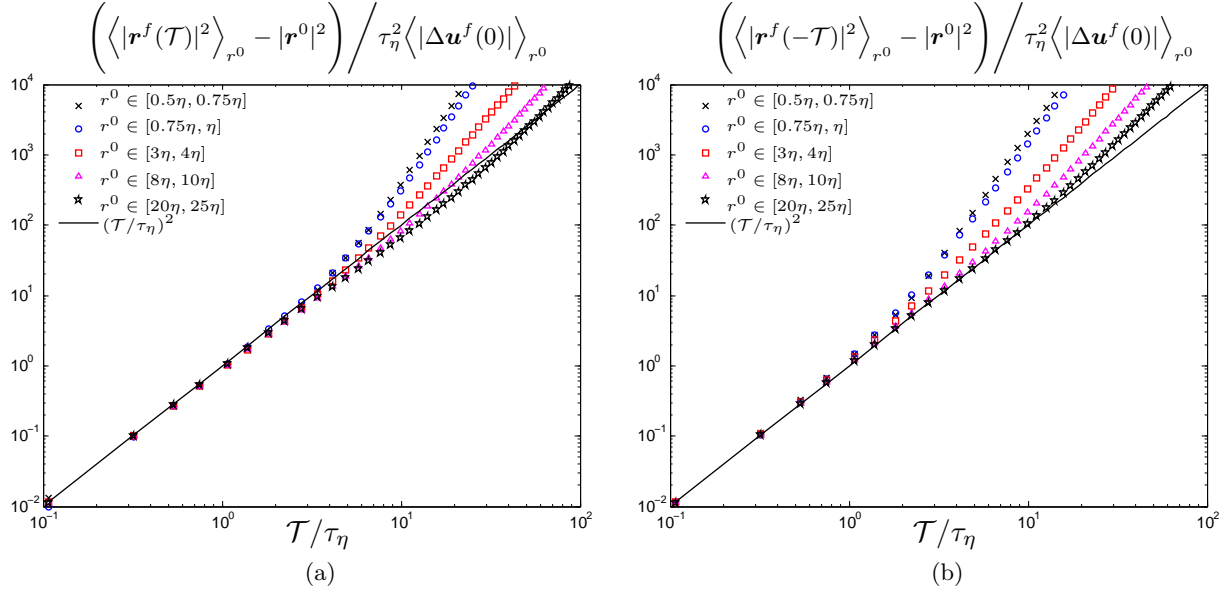


Figure 2: DNS data for (a) FIT and (b) BIT fluid particle mean square separation (with the initial separation subtracted) scaled by  $\tau_\eta^2 \langle |\Delta \mathbf{u}^f(0)| \rangle_{r^0}$ .

Note however that in agreement with Fig. 4 in [13] we find in Fig. 2 (a) that for the larger initial separations the data shows that after an initially ballistic separation the growth then slows down for a time. In Fig. 3 we plot the fluid particle mean square separation (with the initial separation subtracted) scaled by the ballistic prediction and plotted against  $\mathcal{T}/\tau_{r^0}$ , i.e. time scaled by the Batchelor timescale. In agreement with the experimental data in [13] we find in Fig. 3 (a) that for the FIT dispersion the particles begin to separate slower than ballistically for a duration of time after  $\mathcal{T} \sim 0.1\tau_{r^0}$ . The authors in [13] argue that this slowing down is not due to higher order correction terms in the short time series expansion, but argue that it is more likely explained in terms of the effect of the large scales on the separation. In our case the influence of the large scales cannot be the explanation: At these times the particle separations are much smaller than the integral length scale and our data shows a temporary slowing down but then a speeding up towards a faster than ballistic separation (clearly observable in Fig. 3 (a) for  $r^0 \in [8\eta, 10\eta]$  and  $r^0 \in [20\eta, 25\eta]$ ) which cannot be caused by the large scales. A possible explanation for the temporary slowing down of the separation is the effect of the decorrelation of  $\Delta \mathbf{u}^f$  along the pair trajectory (which the ballistic regime neglects through its use of  $\Delta \mathbf{u}^f(s) \approx \Delta \mathbf{u}^f(0)$ ), which is subsequently overcome by the growth of the autocorrelations of  $\Delta \mathbf{u}^f$  in the inertial regime.

The BIT results in Fig. 3 (b) also show the slowing down but to a lesser degree. The BIT data for  $r^0 \in [40\eta, 50\eta]$  and  $r^0 \in [80\eta, 100\eta]$  shows that after the initial ballistic separation their separation slows down, speeds up again to a greater than ballistic separation behavior and then finally slows down again. This final stage of separation is likely due to the large scales since at these times the particle separations exceed the integral length scale, at which the growth follows a diffusive law (corresponding to a line  $\propto \mathcal{T}^{-1}$  in Fig. 3). It is however also possible that at the largest values of  $\mathcal{T}$  the results are affected by the finite box size and periodicity used in the DNS.

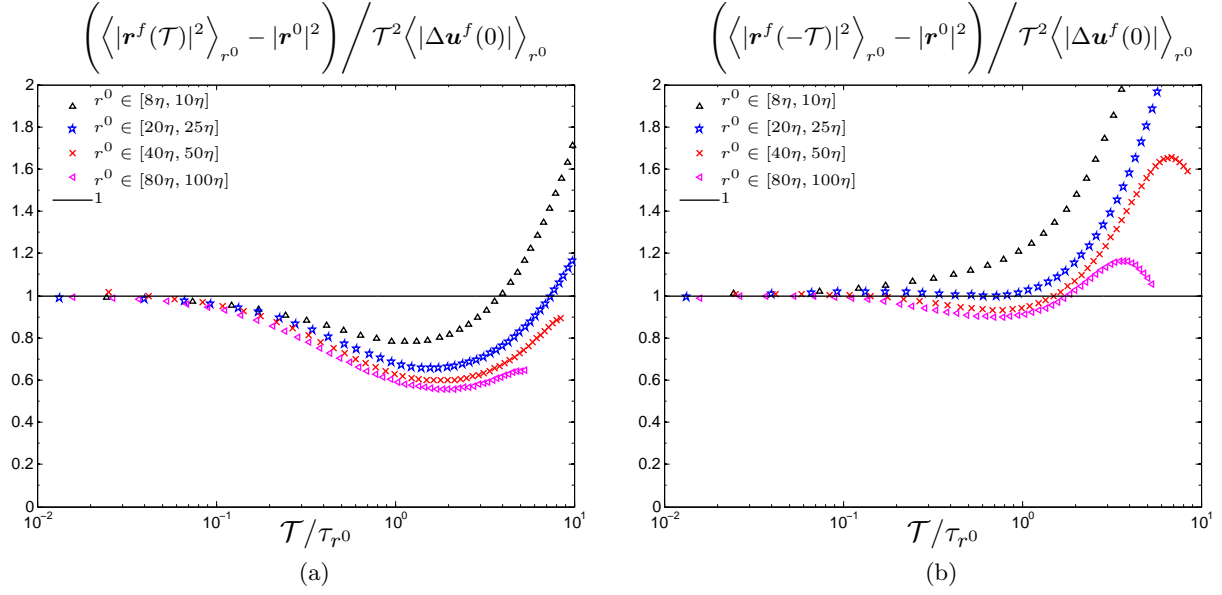


Figure 3: DNS data for (a) FIT and (b) BIT fluid particle mean square separation (with the initial separation subtracted) scaled by the ballistic prediction and plotted against  $\mathcal{T}/\tau_{r^0}$ .

Figure 4 shows the separation of pairs with  $r^0 \leq \eta$ ; symbols represent DNS data and the lines represent theoretical predictions given by (22) and (14) whose color corresponds to the DNS data. The prediction in (22) should be valid provided that the pairs remain in the dissipation regime where the field  $\Delta \mathbf{u}$  is smooth. Our DNS data shows that the statistics of  $\Delta \mathbf{u}$  deviate from the smooth scaling at  $r \sim 10\eta$ . This explains why the predictions from (22) break down at  $\langle |\mathbf{r}^f(\mathcal{T})|^2 \rangle_{r^0} / \eta^2 \sim 100$  for each  $r^0$  in Fig. 4 (a). Once  $\mathbf{r}^f(\mathcal{T}) \gtrsim 10\eta$  their mean square separation goes through a transitory regime, and in  $Re_\lambda \rightarrow \infty$  for sufficiently large  $\mathcal{T}$  they would eventually separate according to the RO law.

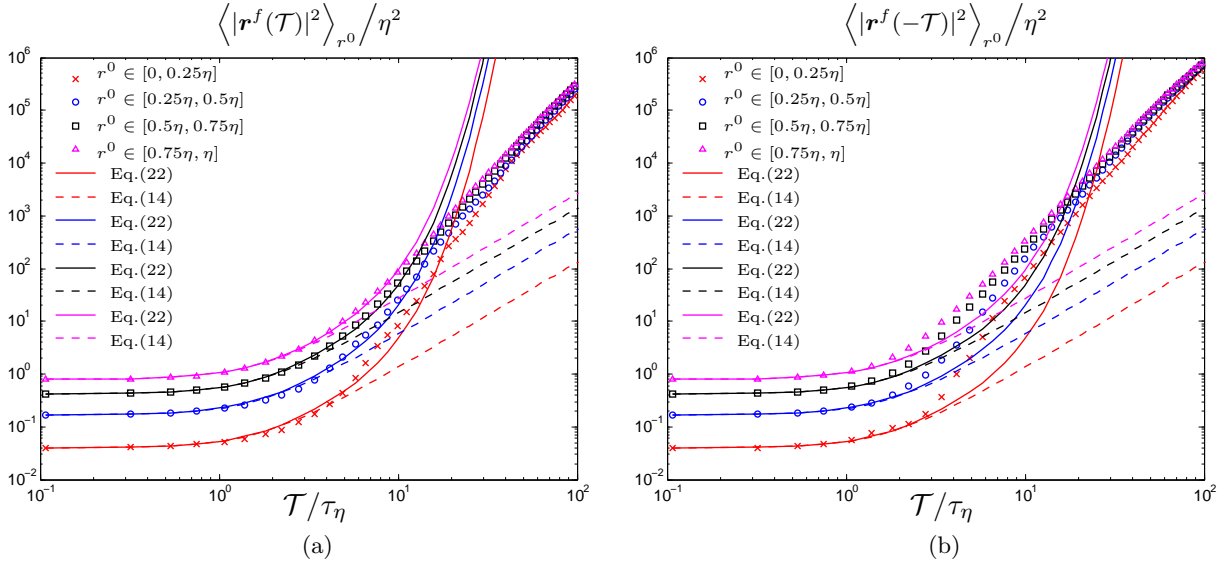


Figure 4: DNS data for (a) FIT and (b) BIT fluid particle mean square separation.

The results in Fig. 4 (b) show that the predictions from (22) and (14) fail to describe the

BIT separation for  $\mathcal{T} \gtrsim \tau_\eta$ . This is not surprising since as discussed earlier, the approximations invoked in deriving (22) and (14) do not capture the effects of time reversal. We may however capture the effects of time reversal as follows. Define  $\tau_\gamma$  as being the timescale associated with the autocovariance

$$\left\langle \left( \mathbf{\Gamma}^f(s) \cdot \mathbf{r}^f(s) \right) \cdot \left( \mathbf{\Gamma}^f(s') \cdot \mathbf{r}^f(s') \right) \right\rangle_{\mathbf{r}^0},$$

in the BIT version of (20). With this timescale, then following a similar procedure to that in deriving (22) we obtain

$$\left\langle |\mathbf{r}^f(-\mathcal{T})|^2 \right\rangle_{\mathbf{r}^0} = |\mathbf{r}^0|^2 + \frac{\langle \epsilon \rangle}{3\nu} |\mathbf{r}^0|^2 \tau_\gamma^2 \left( \exp[\tau_\gamma^{-1} \mathcal{T}] + \exp[-\tau_\gamma^{-1} \mathcal{T}] - 2 \right). \quad (28)$$

Obtaining an analytical estimate for  $\tau_\gamma$  is not feasible, however we can obtain it from the DNS data. This timescale contains, unlike that in (22), the effects of  $\mathbf{r}^f(s) \neq \mathbf{r}^f(s') \neq \mathbf{r}$  (for  $s \neq s' \neq 0$ ), and therefore can capture the faster BIT separation. Figure 5 shows the comparison between the prediction of (28) and the DNS data for the BIT mean square dispersion with  $\tau_\gamma \approx 1.1\tau_\eta$  estimated from the DNS.

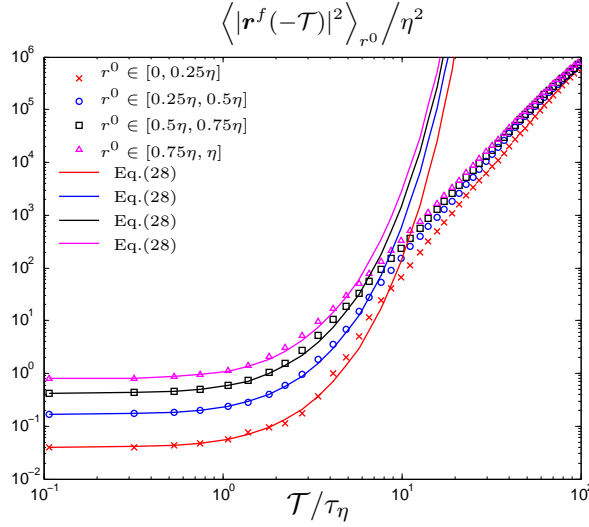


Figure 5: DNS data for BIT fluid particle mean square separation compared with the prediction from (28). The line colors correspond to the DNS data color.

Fig. 5 shows that (28) accurately describes the DNS data up to the time at which  $\langle |\mathbf{r}^f(-\mathcal{T})|^2 \rangle_{\mathbf{r}^0} \sim 100\eta^2$  at which point the theory breaks down for reasons already explained.

For sufficiently large  $\mathcal{T}$ , or for particles with  $r^0$  in the inertial range the mean square separation is predicted to follow the RO  $\mathcal{T}^3$  law. In Fig. 6 we plot  $(\langle |\mathbf{r}^f(\mathcal{T})|^2 \rangle_{\mathbf{r}^0} - |\mathbf{r}^0|^2) / \langle \epsilon \rangle \mathcal{T}^3$  and  $(\langle |\mathbf{r}^f(-\mathcal{T})|^2 \rangle_{\mathbf{r}^0} - |\mathbf{r}^0|^2) / \langle \epsilon \rangle \mathcal{T}^3$  for various  $r^0$  in order to see whether the data shows an approach to RO scaling. For  $r^0 \in [3\eta, 4\eta]$  the data shows a clear convergence to RO scaling in both the FIT and BIT cases, yielding values of  $\mathbf{g}^F$  and  $\mathbf{g}^B$  in excellent agreement with experimental data [17]. For  $r^0 \leq \eta$  the data indicates that for  $\mathcal{T} \gtrsim 5\tau_\eta$  the particles separate faster than RO scaling (indicated by the positive slope for  $\mathcal{T} \gtrsim 5\tau_\eta$ ). We expect this is due to the influence of their separation in the dissipation range because of the finite temporal correlation radius of the field  $\Delta \mathbf{u}$ . For separations larger than  $r^0 \in [3\eta, 4\eta]$  the fluid mean square separation is slower than RO scaling (indicated by the negative slope) throughout the range of  $\mathcal{T}$  for which we have data. The curves do however seem to be tending to RO scaling at the largest values of  $\mathcal{T}$ . For  $r^0$  in the inertial regime we

would expect an initial ballistic separation followed by RO with a transition region in between. For separations larger than  $r^0 \in [3\eta, 4\eta]$  it is likely that our time span of  $0 \leq \mathcal{T} \leq 100\tau_\eta$  only extends to the transition region and hence we do not observe RO scaling. To observe RO scaling over a larger range of  $r^0$  we would need a significantly larger  $Re_\lambda$  DNS. The results in Fig. 6 (a) are very similar to those in Fig. 4 (a) of [19]. Note also that our data agrees with the findings in [20] that  $r^0 \approx 4\eta$  could be an “optimal choice” for the initial separation to observe RO scaling.

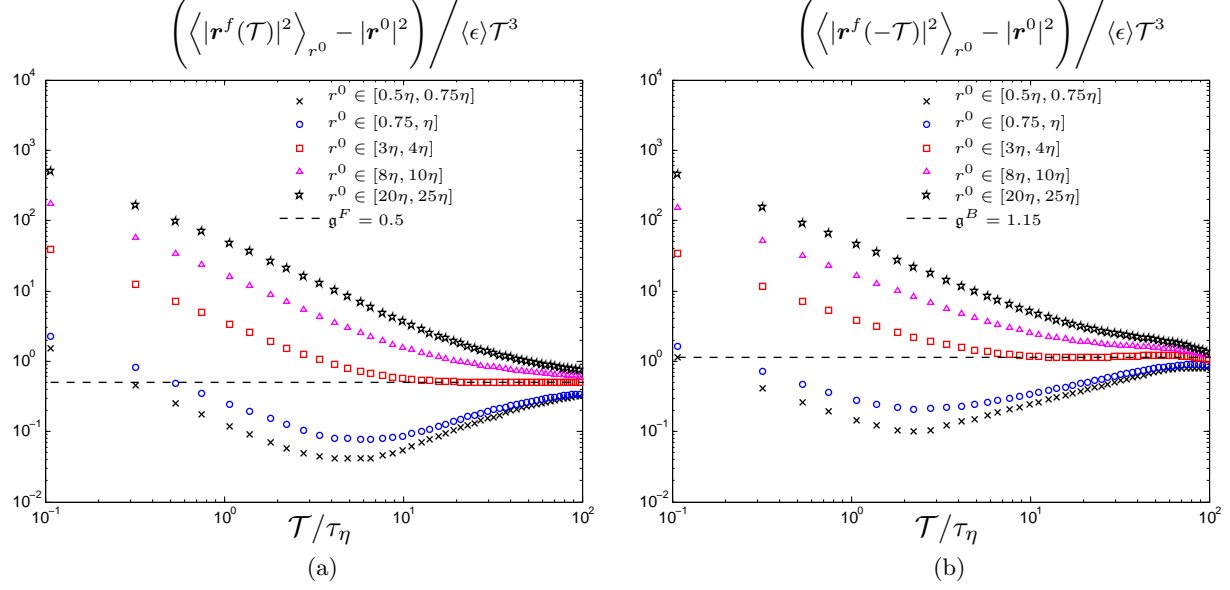


Figure 6: DNS data for (a) FIT and (b) BIT fluid particle mean square separations at various  $r^0$  scaled by  $\langle \epsilon \rangle \mathcal{T}^3$ .

## 4 Inertial particle dispersion

Having considered the dispersion of fluid particles, we now consider the more complex scenario of the dispersion of inertial particles.

### 4.1 Theory

In deriving a theory for the dispersion of inertial particles we will need to know something about the particle relative velocity statistics. In the following, we derive a theory to describe the inertial particle dispersion given only the particle velocity statistics at  $\mathcal{T} = 0$ . The theory then describes, given their statistical state at  $\mathcal{T} = 0$ , how the pairs disperse as a function of  $\mathcal{T}$ . Since the FIT behavior has already been analyzed in [6] we shall focus on developing a theory for the BIT mean square dispersion.

We begin by considering the small  $\mathcal{T}$  limit for which we may invoke the approximation

$$\Delta \mathbf{u}^p(\cdot \cdot \cdot) \approx \Delta \mathbf{u}^p(0),$$

which was also used to derive the fluid particle small time ballistic separation prediction (see §3.1).

Introducing this approximation into (12) and (13) and solving the integrals we obtain

$$\begin{aligned} \left\langle |\mathbf{r}^p(\mathcal{T})|^2 \right\rangle_{\mathbf{r}^0} &\approx |\mathbf{r}^0|^2 + G^2(\mathcal{T}) \left\langle |\mathbf{w}^p(0)|^2 \right\rangle_{\mathbf{r}^0} + 2G(\mathcal{T}) [\mathcal{T} - G(\mathcal{T})] \left\langle \mathbf{w}^p(0) \cdot \Delta \mathbf{u}^p(0) \right\rangle_{\mathbf{r}^0} \\ &+ [\mathcal{T}^2 - 2\mathcal{T}G(\mathcal{T}) + G^2(\mathcal{T})] \left\langle |\Delta \mathbf{u}^p(0)|^2 \right\rangle_{\mathbf{r}^0}, \end{aligned} \quad (29)$$

and

$$\begin{aligned} \left\langle |\mathbf{r}^p(-\mathcal{T})|^2 \right\rangle_{\mathbf{r}^0} &\approx |\mathbf{r}^0|^2 + G^2(\mathcal{T}) \left\langle |\mathbf{w}^p(-\mathcal{T})|^2 \right\rangle_{\mathbf{r}^0} + 2G(\mathcal{T}) [\mathcal{T} - G(\mathcal{T})] \left\langle \mathbf{w}^p(-\mathcal{T}) \cdot \Delta \mathbf{u}^p(0) \right\rangle_{\mathbf{r}^0} \\ &+ [\mathcal{T}^2 - 2\mathcal{T}G(\mathcal{T}) + G^2(\mathcal{T})] \left\langle |\Delta \mathbf{u}^p(0)|^2 \right\rangle_{\mathbf{r}^0}. \end{aligned} \quad (30)$$

For  $\mathbf{r}^0$  in the dissipation regime and  $St \gtrsim 1$  the non-local contribution to the particle pair velocity dynamics gives rise to  $\mathbf{w}^p(0) \gg \Delta \mathbf{u}^p(0)$  [14, 21]. The region in which  $\mathbf{w}^p(0) \gg \Delta \mathbf{u}^p(0)$  shall be referred to as the ‘caustic region’. In the caustic regions (29) and (30) reduce to

$$\left\langle |\mathbf{r}^p(\mathcal{T})|^2 \right\rangle_{\mathbf{r}^0} \approx |\mathbf{r}^0|^2 + G^2(\mathcal{T}) \left\langle |\mathbf{w}^p(0)|^2 \right\rangle_{\mathbf{r}^0}, \quad (31)$$

$$\left\langle |\mathbf{r}^p(-\mathcal{T})|^2 \right\rangle_{\mathbf{r}^0} \approx |\mathbf{r}^0|^2 + G^2(\mathcal{T}) \left\langle |\mathbf{w}^p(-\mathcal{T})|^2 \right\rangle_{\mathbf{r}^0}, \quad (32)$$

and the FIT result in (31) is a result previously derived in [6]. Since particle pairs were on average at larger separations in the past (i.e.  $\langle |\mathbf{r}^p(-\mathcal{T})|^2 \rangle_{\mathbf{r}^0} \geq |\mathbf{r}^0|^2$ ), then  $\langle |\mathbf{w}^p(-\mathcal{T})|^2 \rangle_{\mathbf{r}^0} \geq \langle |\mathbf{w}^p(0)|^2 \rangle_{\mathbf{r}^0}$ . Consequently in the caustic regions the pair dispersion is time-irreversible with BIT dispersion occurring at a faster rate than FIT dispersion. This feature is universal in the sense that it does not depend upon any time-irreversibility in the fluid flow dynamics and would therefore exist even in time-reversible flows such as Kinematic Simulation (KS).

The physical mechanism giving rise to the time-irreversibility of inertial particle dispersion is explained as follows: In FIT dispersion, since the particle pairs on average separate, they retain a memory of smaller fluid velocity differences in their path history. However in BIT dispersion, particle pairs are on average approaching one another and so retain a memory of larger fluid velocity differences in their path history. A memory of larger scale turbulent motions in BIT dispersion, compared to a memory of smaller scale turbulent motions in FIT dispersion breaks the FIT/BIT symmetry and gives rise to faster BIT dispersion than FIT. We expect that the degree of time-irreversibility will be maximum for  $\tau_p/\tau_{r^0} \sim 1$  since such particles are strongly affected by both the time-irreversibility of the turbulence and that arising from the history effect of their inertia. Note that this path history symmetry breaking mechanism vanishes for particle separations at the integral scales because at those scales the statistics of  $\Delta \mathbf{u}$  become independent of separation, ensuring that at these scales the pair dispersion becomes time-reversible.

We now must verify that the results in (29) and (30) obey the necessary limiting case. First, it is simple to confirm that (29) and (30) reduce to (14) in the case when  $\tau_p = 0$ . Second, in a  $Re_\lambda \rightarrow \infty$  turbulent flow then for sufficiently large  $\mathbf{r}^0$  the inertial particle behavior should tend to that for fluid particles since for a given  $\tau_p$ ,  $\tau_p/\tau_{r^0} \rightarrow 0$  as  $|\mathbf{r}^0| \rightarrow \infty$ . In this limit, for arbitrary finite  $\tau_p$  at sufficiently large  $\mathbf{r}^0$  we would have  $\mathbf{w}^p \rightarrow \Delta \mathbf{u}^f$ ; if we introduce this limit into (29) and (30) we once again find that the results reduce to (14).

The result in (30) however contains  $\mathbf{w}^p(-\mathcal{T})$ ; we wish to derive theoretical descriptions that require only knowledge of the particle velocity statistics at  $\mathcal{T} = 0$ . The solution for  $\mathbf{w}^p(-\mathcal{T})$  is

$$\mathbf{w}^p(-\mathcal{T}) = \dot{G}^{-1}(\mathcal{T}) \mathbf{w}^p(0) - \tau_p^{-1} \dot{G}^{-1}(\mathcal{T}) \int_{-\mathcal{T}}^0 \dot{G}(-s) \Delta \mathbf{u}^p(s) ds, \quad (33)$$

where  $\dot{G}(-s) = \exp[\tau_p^{-1}s]$ . From (33) we obtain the following

$$\begin{aligned} \left\langle |\mathbf{w}^p(-\mathcal{T})|^2 \right\rangle_{\mathbf{r}^0} &= \dot{G}^{-2}(\mathcal{T}) \left\langle |\mathbf{w}^p(0)|^2 \right\rangle_{\mathbf{r}^0} - 2\tau_p^{-1} \dot{G}^{-2}(\mathcal{T}) \int_{-\mathcal{T}}^0 \dot{G}(-s) \left\langle \mathbf{w}^p(0) \cdot \Delta \mathbf{u}^p(s) \right\rangle_{\mathbf{r}^0} ds \\ &\quad + \tau_p^{-2} \dot{G}^{-2}(\mathcal{T}) \int_{-\mathcal{T}}^0 \int_{-\mathcal{T}}^0 \dot{G}(-s) \dot{G}(-s') \left\langle \Delta \mathbf{u}^p(s) \cdot \Delta \mathbf{u}^p(s') \right\rangle_{\mathbf{r}^0} ds' ds. \end{aligned} \quad (34)$$

Introducing into this  $\Delta \mathbf{u}^p(s) \approx \Delta \mathbf{u}^p(0)$  and evaluating the integrals we obtain

$$\begin{aligned} \left\langle |\mathbf{w}^p(-\mathcal{T})|^2 \right\rangle_{\mathbf{r}^0} &\approx \dot{G}^{-2}(\mathcal{T}) \left\langle \mathbf{w}^p(0) \cdot \mathbf{w}^p(0) \right\rangle_{\mathbf{r}^0} - 2\tau_p^{-1} \dot{G}^{-2}(\mathcal{T}) G(\mathcal{T}) \left\langle \mathbf{w}^p(0) \cdot \Delta \mathbf{u}^p(0) \right\rangle_{\mathbf{r}^0} \\ &\quad + \tau_p^{-2} \dot{G}^{-2}(\mathcal{T}) G^2(\mathcal{T}) \left\langle \Delta \mathbf{u}^p(0) \cdot \Delta \mathbf{u}^p(0) \right\rangle_{\mathbf{r}^0}. \end{aligned} \quad (35)$$

In a similar manner we also obtain

$$\left\langle \mathbf{w}^p(-\mathcal{T}) \cdot \Delta \mathbf{u}^p(0) \right\rangle_{\mathbf{r}^0} \approx \dot{G}^{-1}(\mathcal{T}) \left\langle \mathbf{w}^p(0) \cdot \Delta \mathbf{u}^p(0) \right\rangle_{\mathbf{r}^0} - \tau_p^{-1} \dot{G}^{-1}(\mathcal{T}) G(\mathcal{T}) \left\langle \Delta \mathbf{u}^p(0) \cdot \Delta \mathbf{u}^p(0) \right\rangle_{\mathbf{r}^0}. \quad (36)$$

Using these results in (30) we obtain

$$\begin{aligned} \left\langle |\mathbf{r}^p(-\mathcal{T})|^2 \right\rangle_{\mathbf{r}^0} &\approx |\mathbf{r}^0|^2 + G^2(-\mathcal{T}) \left\langle |\mathbf{w}^p(0)|^2 \right\rangle_{\mathbf{r}^0} - 2G(-\mathcal{T}) \left( G(-\mathcal{T}) + \mathcal{T} \right) \left\langle \mathbf{w}^p(0) \cdot \Delta \mathbf{u}^p(0) \right\rangle_{\mathbf{r}^0} \\ &\quad + \left[ G^2(-\mathcal{T}) + 2\mathcal{T}G(-\mathcal{T}) + \mathcal{T}^2 \right] \left\langle |\Delta \mathbf{u}^p(0)|^2 \right\rangle_{\mathbf{r}^0}. \end{aligned} \quad (37)$$

In addition, since we do not in general know the statistics of  $\Delta \mathbf{u}^p$  we make the approximation

$$\left\langle |\Delta \mathbf{u}^p(0)|^2 \right\rangle_{\mathbf{r}^0} \approx \left\langle |\Delta \mathbf{u}^f(0)|^2 \right\rangle_{\mathbf{r}^0}, \quad (38)$$

and also

$$\left\langle \mathbf{w}^p(0) \cdot \Delta \mathbf{u}^p(0) \right\rangle_{\mathbf{r}^0} \approx \sqrt{\left\langle |\mathbf{w}^p(0)|^2 \right\rangle_{\mathbf{r}^0}} \sqrt{\left\langle |\Delta \mathbf{u}^f(0)|^2 \right\rangle_{\mathbf{r}^0}}, \quad (39)$$

which finally gives us

$$\begin{aligned} \left\langle |\mathbf{r}^p(-\mathcal{T})|^2 \right\rangle_{\mathbf{r}^0} &\approx |\mathbf{r}^0|^2 + G^2(-\mathcal{T}) \left\langle |\mathbf{w}^p(0)|^2 \right\rangle_{\mathbf{r}^0} + \left[ G^2(-\mathcal{T}) + 2\mathcal{T}G(-\mathcal{T}) + \mathcal{T}^2 \right] \left\langle |\Delta \mathbf{u}^f(0)|^2 \right\rangle_{\mathbf{r}^0} \\ &\quad - 2G(-\mathcal{T}) \left( G(-\mathcal{T}) + \mathcal{T} \right) \sqrt{\left\langle |\mathbf{w}^p(0)|^2 \right\rangle_{\mathbf{r}^0}} \sqrt{\left\langle |\Delta \mathbf{u}^f(0)|^2 \right\rangle_{\mathbf{r}^0}}. \end{aligned} \quad (40)$$

We have therefore derived a general result for the BIT dispersion of inertial particles at short times, which is valid for all  $\tau_p$  and which exhibits the correct behavioral variation with  $\mathbf{r}^0$  for a given  $\tau_p$ .

It is possible that (40) may not be accurate for small  $St$  since by invoking approximation (38) we have partially removed the effect of the preferential sampling of  $\Delta \mathbf{u}$  by the inertial particles (some of the effect is captured within  $\left\langle |\mathbf{w}^p(0)|^2 \right\rangle_{\mathbf{r}^0}$ ). We consider the effects of this on (40) for low  $St$  particles in §4.2.

For inertial particles in caustic regions we expect that the small  $\mathcal{T}$  prediction is accurate up to  $\mathcal{T} \sim \tau_p$  since this is approximately the time it takes for the particles to relax to the turbulent motions

of the fluid. For fluid particles the ballistic motion persists for times of the order of  $\tau_{r^0}$ , i.e. the Batchelor time. We may therefore expect that (40) is appropriate for  $\mathcal{T} \lesssim \max[\tau_p, \tau_{r^0}]$ . For initial separations in the dissipation regime we take  $\tau_{r^0} = \tau_\eta$  and in the inertial range  $\tau_{r^0} = (|\mathbf{r}^0|^2/\langle\epsilon\rangle)^{1/3}$ .

Having considered the dispersion of particles for  $\mathcal{T} \lesssim \max[\tau_p, \tau_{r^0}]$ , we now consider the regime  $\mathcal{T} > \max[\tau_p, \tau_{r^0}]$ . Once again, ignoring the mean terms, we may re-write (13) for  $\mathcal{T} > \hat{\mathcal{T}}$  as

$$\begin{aligned}
\left\langle |\mathbf{r}^p(-\mathcal{T})|^2 \right\rangle_{\mathbf{r}^0} &= |\mathbf{r}^0|^2 + G^2(\hat{\mathcal{T}}) \left\langle \mathbf{w}^p(-\hat{\mathcal{T}}) \cdot \mathbf{w}^p(-\hat{\mathcal{T}}) \right\rangle_{\mathbf{r}^0} \\
&+ 2\tau_p^{-1} G(\hat{\mathcal{T}}) \int_{-\hat{\mathcal{T}}}^0 G(-s) \left\langle \mathbf{w}^p(-\hat{\mathcal{T}}) \cdot \Delta \mathbf{u}^p(s) \right\rangle_{\mathbf{r}^0} ds \\
&+ \tau_p^{-2} \int_{-\hat{\mathcal{T}}}^0 \int_{-\hat{\mathcal{T}}}^0 G(-s) G(-s') \left\langle \Delta \mathbf{u}^p(s) \cdot \Delta \mathbf{u}^p(s') \right\rangle_{\mathbf{r}^0} ds' ds \\
&- \int_{-\mathcal{T}}^{-\hat{\mathcal{T}}} \frac{d}{ds} \left[ G^2(-s) \left\langle \mathbf{w}^p(s) \cdot \mathbf{w}^p(s) \right\rangle_{\mathbf{r}^0} \right] ds \\
&+ 2\tau_p^{-1} G(\mathcal{T}) \int_{-\mathcal{T}}^{-\hat{\mathcal{T}}} G(-s) \left\langle \mathbf{w}^p(-\mathcal{T}) \cdot \Delta \mathbf{u}^p(s) \right\rangle_{\mathbf{r}^0} ds \\
&+ \tau_p^{-2} \int_{-\mathcal{T}}^{-\hat{\mathcal{T}}} \int_{-\mathcal{T}}^{-\hat{\mathcal{T}}} G(-s) G(-s') \left\langle \Delta \mathbf{u}^p(s) \cdot \Delta \mathbf{u}^p(s') \right\rangle_{\mathbf{r}^0} ds' ds,
\end{aligned} \tag{41}$$

where  $\hat{\mathcal{T}} = \max[\tau_p, \tau_{r^0}]$ . The solution to the first three lines in (41) is given by (40) evaluated at  $\mathcal{T} = \hat{\mathcal{T}}$ ; the task now is to derive approximate analytical solutions for the last three lines in (41).

Determining the appropriate closure approximations to apply to the last three lines in (41) depends upon both  $St$  and  $r^0$ . For example, for  $r^0 \ll \eta$  then depending upon the value of  $St$  the particles may be either still in the dissipation regime or in the inertial regime at time  $\hat{\mathcal{T}}$ . If they are still in the dissipation regime then they may begin (depending on  $St$ ) to separate exponentially because of the smooth turbulent velocity difference field at these scales. However if they are in the inertial regime at time  $\hat{\mathcal{T}}$  then they may begin to separate with an RO type growth (this was found for the FIT separation in the large time regime [6]). We will assume that at time  $\hat{\mathcal{T}}$  the pairs are in the inertial regime and leave the other case for future work.

Let us define the scale dependent  $St$  number as  $St(r) = \tau_p/\tau_r$ , where  $\tau_r$  is the Lagrangian timescale associated with  $\Delta \mathbf{u}$  at separation  $r = |\mathbf{r}|$ . If we have  $St(r \sim \eta) \sim 1$  then because  $\tau_r$  grows with  $r$ ,  $St(r \gg \eta) \ll 1$  implying that as the particles separate to larger and larger scales the effect of their inertia becomes perturbative, i.e.  $\mathbf{w}^p \approx \Delta \mathbf{u}^p$ . We will make the approximation that  $\mathbf{w}^p \approx \Delta \mathbf{u}^p$  for  $\mathcal{T} > \hat{\mathcal{T}}$ . With this approximation, and assuming, as discussed previously, that for  $\mathcal{T} > \hat{\mathcal{T}}$  the pairs are in the inertial range, we may use K41 type arguments to obtain the following



closures (note that in (41),  $s$  and  $s'$  are evaluated at negative times)

$$\left\langle |\mathbf{w}^p(s)|^2 \right\rangle_{\mathbf{r}^0} \approx -\mathcal{A}\langle\epsilon\rangle s, \quad (42)$$

$$\left\langle \mathbf{w}^p(-\mathcal{T}) \cdot \Delta \mathbf{u}^p(s) \right\rangle_{\mathbf{r}^0} \approx -\mathcal{A}\langle\epsilon\rangle (1/2)(s - \mathcal{T}), \quad (43)$$

$$\left\langle \Delta \mathbf{u}^p(s) \cdot \Delta \mathbf{u}^p(s') \right\rangle_{\mathbf{r}^0} \approx -\mathcal{A}\langle\epsilon\rangle (1/2)(s + s'). \quad (44)$$

If we now substitute these into (41) and take  $G(\mathcal{T} > \hat{\mathcal{T}}) \approx \tau_p$  then the solution is

$$\begin{aligned} \left\langle |\mathbf{r}^p(-\mathcal{T})|^2 \right\rangle_{\mathbf{r}^0} &\approx \left\langle |\mathbf{r}^p(-\hat{\mathcal{T}})|^2 \right\rangle_{\mathbf{r}^0} + \tau_p^2 \mathcal{A}\langle\epsilon\rangle (\mathcal{T} - \hat{\mathcal{T}}) - \tau_p (1/2) \mathcal{A}\langle\epsilon\rangle (\hat{\mathcal{T}}^2 + 2\hat{\mathcal{T}}\mathcal{T} - 3\mathcal{T}^2) \\ &\quad + (1/2) \mathcal{A}\langle\epsilon\rangle (\mathcal{T}^3 + \hat{\mathcal{T}}^3 - \hat{\mathcal{T}}^2\mathcal{T} - \hat{\mathcal{T}}\mathcal{T}^2), \quad \text{for } \mathcal{T} > \hat{\mathcal{T}}, \end{aligned} \quad (45)$$

where again in this expression  $\langle |\mathbf{r}^p(-\hat{\mathcal{T}})|^2 \rangle_{\mathbf{r}^0}$  is given by (40) evaluated at  $\mathcal{T} = \hat{\mathcal{T}}$ . Taking the limit  $\tau_p \rightarrow 0$  and  $\mathcal{T} \gg \hat{\mathcal{T}}$  we may identify  $(1/2)\mathcal{A}$  in (45) as the backward in time Richardson constant  $\mathbf{g}^B$  and therefore write (45) as

$$\begin{aligned} \left\langle |\mathbf{r}^p(-\mathcal{T})|^2 \right\rangle_{\mathbf{r}^0} &\approx \left\langle |\mathbf{r}^p(-\hat{\mathcal{T}})|^2 \right\rangle_{\mathbf{r}^0} + 2\tau_p^2 \mathbf{g}^B\langle\epsilon\rangle (\mathcal{T} - \hat{\mathcal{T}}) - \tau_p \mathbf{g}^B\langle\epsilon\rangle (\hat{\mathcal{T}}^2 + 2\hat{\mathcal{T}}\mathcal{T} - 3\mathcal{T}^2) \\ &\quad + \mathbf{g}^B\langle\epsilon\rangle (\mathcal{T}^3 + \hat{\mathcal{T}}^3 - \hat{\mathcal{T}}^2\mathcal{T} - \hat{\mathcal{T}}\mathcal{T}^2), \quad \text{for } \mathcal{T} > \hat{\mathcal{T}}, \end{aligned} \quad (46)$$

which correctly tends to  $\mathbf{g}^B\langle\epsilon\rangle\mathcal{T}^3$  for  $\mathcal{T} \gg \hat{\mathcal{T}}$ . For fluid particles  $\mathbf{g}^B$  is known ( $\approx 1.15$ ), however for inertial particles its value is unknown. Therefore we must regard this as a tuning parameter (although the tuning is not entirely arbitrary since we know its value for  $St = 0$ , about which the inertial particle value will be perturbed). However, in §4.2 we show that in some cases this constant can be obtained from DNS data.

Earlier we verified that the short time theory in (40) satisfies the correct behavioral variation with  $\mathbf{r}^0$ , namely, for a given finite  $St$  at sufficiently large  $\mathbf{r}^0$  the pair should separate as fluid particles. We now confirm that (46) also has the correct behavior. Consider  $St(r \sim \eta) \sim 1$  and  $\eta \ll |\mathbf{r}^0| \ll L$ . Recall that  $\hat{\mathcal{T}} = \max[\tau_p, \tau_{r^0}]$ : For  $\eta \ll |\mathbf{r}^0| \ll L$  then  $\tau_{r^0} \sim (|\mathbf{r}^0|^2/\langle\epsilon\rangle)^{1/3}$  and with  $St \sim 1$  we therefore have  $\tau_p \ll \hat{\mathcal{T}}$  and thus for  $\mathcal{T} > \hat{\mathcal{T}}$

$$\begin{aligned} &2\tau_p^2 \mathbf{g}^B\langle\epsilon\rangle (\mathcal{T} - \hat{\mathcal{T}}) - \tau_p \mathbf{g}^B\langle\epsilon\rangle (\hat{\mathcal{T}}^2 + 2\hat{\mathcal{T}}\mathcal{T} - 3\mathcal{T}^2) + \mathbf{g}^B\langle\epsilon\rangle (\mathcal{T}^3 + \hat{\mathcal{T}}^3 - \hat{\mathcal{T}}^2\mathcal{T} - \hat{\mathcal{T}}\mathcal{T}^2) \\ &\rightarrow \mathbf{g}^B\langle\epsilon\rangle (\mathcal{T}^3 + \tau_{r^0}^3 - \tau_{r^0}^2\mathcal{T} - \tau_{r^0}\mathcal{T}^2). \end{aligned}$$

Therefore (46) satisfies the condition that for finite  $St$  the effects of particle inertia vanish for sufficiently large  $\mathbf{r}^0$  in  $Re_\lambda \rightarrow \infty$  turbulence, and tends to the BIT RO result for large  $\mathcal{T}$ .

Finally, note that by its essentially perturbative construction, (46) is, like the fluid particle RO law, free from intermittency corrections since it depends linearly upon the energy dissipation of the fluid [22–24].

## 4.2 DNS results

Before considering the results for the particle pair mean square separation we first present the DNS data for  $\langle |\mathbf{w}^p(0)|^2 \rangle_{\mathbf{r}^0}$  which will be useful when considering the dispersion results, and also because this statistic features in the small time theory (40). Since we are considering an isotropic system the statistics depend only upon on the separation magnitude  $r^0 = |\mathbf{r}^0|$ .

Comparing the  $St > 0$  results in Figure 7 with the fluid particle results ( $St = 0$ , for which  $\langle |\mathbf{w}^p(0)|^2 \rangle_{\mathbf{r}^0} = \langle |\mathbf{u}^f(0)|^2 \rangle_{\mathbf{r}^0}$ ) we see that at larger separations the particle inertia gives rise to

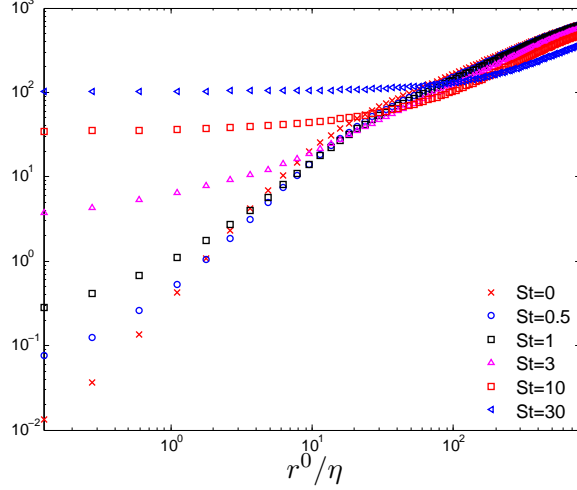


Figure 7: DNS data for  $\langle |\mathbf{w}^p(0)|^2 \rangle_{r^0} / u_\eta^2$  as a function of  $r^0 / \eta$  for various  $St$ .

$\langle |\mathbf{w}^p(0)|^2 \rangle_{r^0} < \langle |\mathbf{u}^f(0)|^2 \rangle_{r^0}$  whereas at the smaller separations  $\langle |\mathbf{w}^p(0)|^2 \rangle_{r^0} > \langle |\mathbf{u}^f(0)|^2 \rangle_{r^0}$ . The separation at which the transition in behavior occurs is a strong function of  $St$ . For a detailed explanation of the role of inertia on these statistics see [10,14], here we summarize. The predominant effects of inertia at these  $St$  numbers are the filtering and non-local effects (preferential sampling of  $\Delta \mathbf{u}$  has a role mainly for  $0 < St \lesssim 0.4$  and in the dissipation range [14]). The inertia of the particles causes them to filter out the high frequency fluctuations of  $\Delta \mathbf{u}$ , and since the inertia gives the particles a memory, their velocity dynamics at a given separation may be strongly influenced by their path history interactions with the turbulent velocity field. For a given  $\tau_p$  the non-local contribution becomes less important as one goes to larger and larger separations so that the filtering effect dominates; this gives rise to  $\langle |\mathbf{w}^p(0)|^2 \rangle_{r^0} < \langle |\mathbf{u}^f(0)|^2 \rangle_{r^0}$ . At the smaller scales the non-local effect of inertia dominates which gives rise to  $\langle |\mathbf{w}^p(0)|^2 \rangle_{r^0} > \langle |\mathbf{u}^f(0)|^2 \rangle_{r^0}$ .

Fig. 8 shows results for  $\langle |\mathbf{r}^p(\mathcal{T})|^2 \rangle_{r^0}$  and  $\langle |\mathbf{r}^p(-\mathcal{T})|^2 \rangle_{r^0}$  from DNS for  $r^0 \in [0.25\eta, 0.5\eta]$ ,  $r^0 \in [3\eta, 4\eta]$  and various  $St$ . Comparing the FIT and BIT results, it is apparent that strong qualitative differences are present in addition to significant quantitative differences.

The FIT dispersion is explained as follows: For small  $r^0$  and sufficiently large  $St$  the inertial particles initially separate much faster than the fluid particles owing to the presence of caustics in their relative velocities at small  $r^0$ , giving rise to  $\mathbf{w}^p \gg \Delta \mathbf{u}^p$  (see Fig. 7). This continues up to  $\mathcal{T} \sim \tau_p$  after which the fluid velocity field begins to significantly affect their motion, and after a few multiples of  $\tau_p$  the fluid particles overtake because they are now separating faster than the inertial particles. The inertial particle separation begins to lag behind the fluid particles for two reasons: First, inertia filters out high frequency modes of  $\Delta \mathbf{u}^p$  [14] and second, because the particles are on average separating they carry a memory of smaller fluid velocity differences in their path history. Consequently if we consider a set of inertial particles with a range of  $\tau_p$ , then for  $\mathcal{T} \gg \max[\tau_p]$ ,  $\langle |\mathbf{r}^p(\mathcal{T})|^2 \rangle_{r^0}$  decreases with increasing  $\tau_p$ . This behavior is observable in Fig. 8 (c).

The BIT behavior is explained as follows: As shown in Fig. 7, at large separations the particle relative velocities decrease relative to the fluid with increasing  $St$ . Consequently for very large  $\mathcal{T}$ , corresponding to pairs at large scale separations, the rate at which particle pairs were approaching each other decreased as  $St$  increased (the  $\mathcal{T}$  range in our DNS data is too limited to observe this). However, as the particle pairs begin to enter the inertial range the fluid velocity differences

they experience begin to decrease (statistically) and the rate of approach for fluid particle pairs decreases. Since inertial particles have a memory, however, when they are in the inertial range they will be still carrying a memory of their interaction with larger scale turbulent motions in their path history and hence at some separation and time  $\mathcal{T}$  they begin to decouple from the fluid turbulence and approach each other with greater relative velocities than the fluid particle pairs. Because BIT separating pairs retain, on average, a memory of larger scale fluid velocity differences in their path history they approach each other faster than the fluid particles not only at short times but also at intermediate times, contrasted with the FIT case as discussed earlier. Thus the particles memory of their path history interactions with the turbulence not only gives rise to faster BIT than FIT separation, but also gives rise to qualitative differences in their separation.

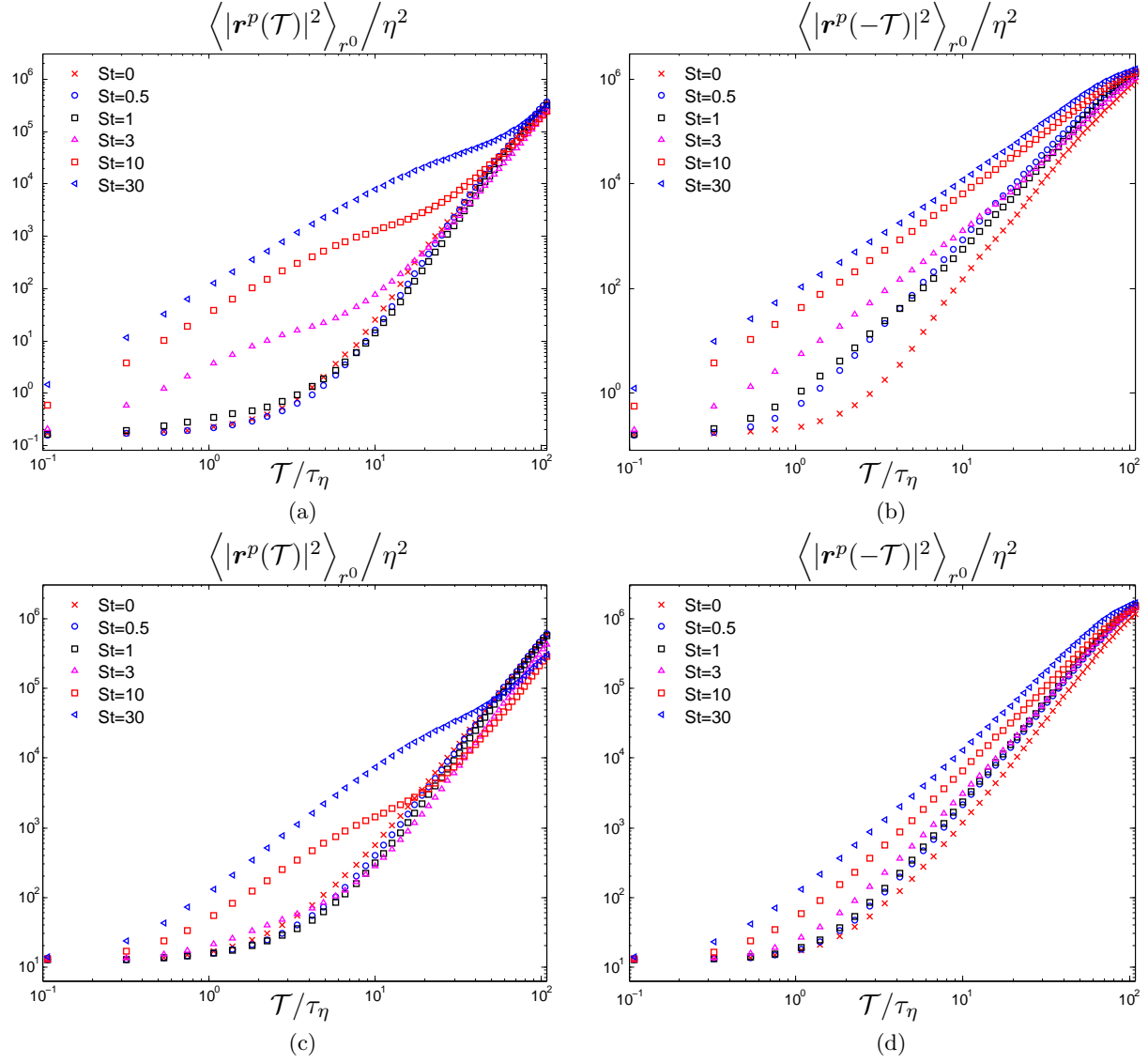


Figure 8: FIT and BIT mean square separation results from DNS for (a),(b)  $r^0 \in [0.25\eta, 0.5\eta]$  and (c),(d)  $r^0 \in [3\eta, 4\eta]$  and various  $St$ .

This explanation for the qualitative differences between FIT and BIT separation is supported by considering the behavior of the inertial particle mean square relative velocities in Fig. 9.

Notice the striking difference in the FIT and BIT relative velocities shown in Fig. 9, with

$\langle |\mathbf{w}^p(\mathcal{T})|^2 \rangle_{r^0}$  decreasing for  $\mathcal{T} \lesssim \tau_p$  and  $\langle |\mathbf{w}^p(-\mathcal{T})|^2 \rangle_{r^0}$  increasing for  $\mathcal{T} \lesssim \tau_p$ . This may be explained by considering the evolution equations for the respective quantities. In the caustic regions and for  $\mathcal{T} \lesssim \tau_p$  we have

$$\langle |\mathbf{w}^p(\mathcal{T})|^2 \rangle_{r^0} \approx \dot{G}^2(\mathcal{T}) \langle |\mathbf{w}^p(0)|^2 \rangle_{r^0} = \exp \left[ -2\tau_p^{-1} \mathcal{T} \right] \langle |\mathbf{w}^p(0)|^2 \rangle_{r^0}, \quad (47)$$

$$\langle |\mathbf{w}^p(-\mathcal{T})|^2 \rangle_{r^0} \approx \dot{G}^{-2}(\mathcal{T}) \langle |\mathbf{w}^p(0)|^2 \rangle_{r^0} = \exp \left[ 2\tau_p^{-1} \mathcal{T} \right] \langle |\mathbf{w}^p(0)|^2 \rangle_{r^0}. \quad (48)$$

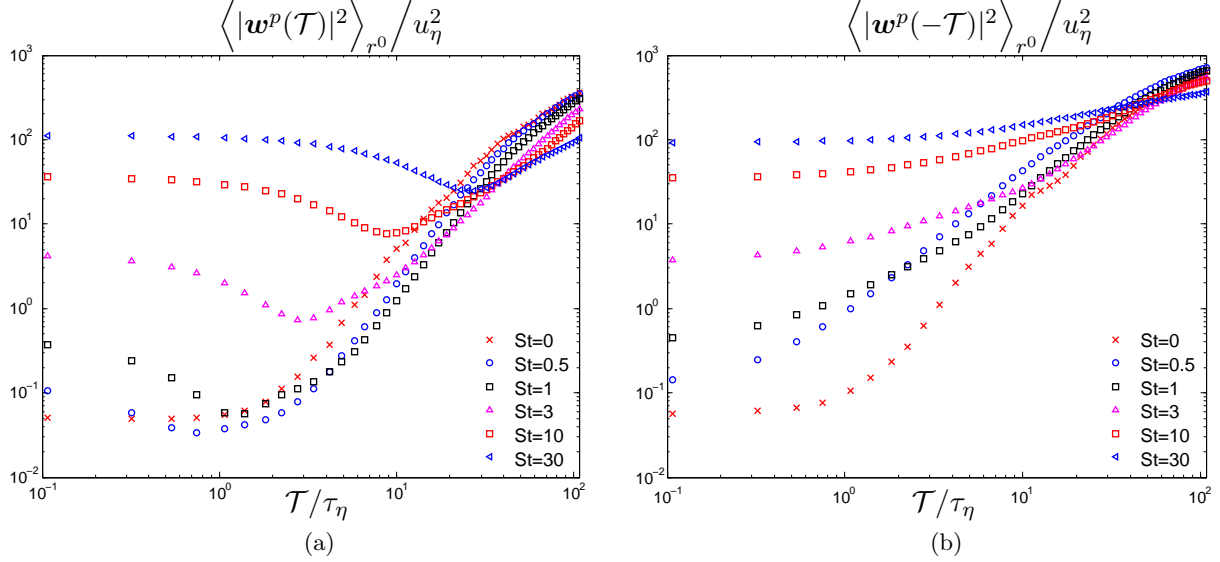


Figure 9: FIT (a) and BIT (b) mean square relative velocity results from DNS for  $r^0 \in [0.25\eta, 0.5\eta]$  and various  $St$ .

In the FIT case the inertial particles separate for  $\mathcal{T} \lesssim \tau_p$  according with their initial velocities, and begin to slow down due to the drag of the fluid. In the BIT case the inertial particles are also slowing down as they approach each other, which when viewed BIT gives the appearance of the particles speeding up. In general the FIT and BIT mean square velocity difference behavior differs with  $\mathcal{T}$  because in the FIT case the pairs carry a memory of smaller fluid velocity differences whereas in BIT the pairs carry a memory of larger fluid velocity differences in their path history. This difference in the behavior of the particle relative velocities FIT and BIT with increasing  $\mathcal{T}$  is responsible for the qualitative differences between the FIT and BIT mean square separation discussed previously.

In order to show the effects of time reversal more clearly in Figure 10 (a)-(c) we plot the ratio of the BIT to FIT mean square separation for various  $r^0$  and  $St$ . The results clearly show that  $\max[\langle |\mathbf{r}^p(-\mathcal{T})|^2 \rangle_{r^0} / \langle |\mathbf{r}^p(\mathcal{T})|^2 \rangle_{r^0}]$  is a strong function of  $St$  and  $r^0$ , with the effect of time-reversal being much greater for inertial particles than for fluid particles. This is for the reason explained in §4.1, namely, that inertial particles experience an additional source of time-irreversibility because of the difference in their path history interactions with the turbulence when separating FIT and BIT. At each  $r^0$  there is an optimum value of  $St$  for which the time-irreversibility is greatest, and it corresponds to the value for which the particles experience optimally both the time-irreversibility of the turbulence and also that arising because of the history effect of the particle inertia. As  $r^0$  is increased, this optimum value of  $St$  increases because the effects of inertia (for a given  $\tau_p$ ) decrease with increasing separation. For  $r^0 > L$  the FIT and BIT dispersion become equivalent,

and becomes related to the one particle dispersion problem since the motion of the two particles at such separations is uncorrelated. The single particle dispersion should be time reversible in stationary isotropic turbulence since the large scale motions of the turbulence (which dominate the single particle dispersion) are approximately time reversible and because there is no path history symmetry breaking mechanism arising from inertia since the field  $\mathbf{u}$  is homogeneous and isotropic. The results in Figure 10 (d) for the single particle dispersion in the DNS confirm this expectation (where  $\mathbf{x}^p(t)$  is the position of a single particle at time  $t$ ).

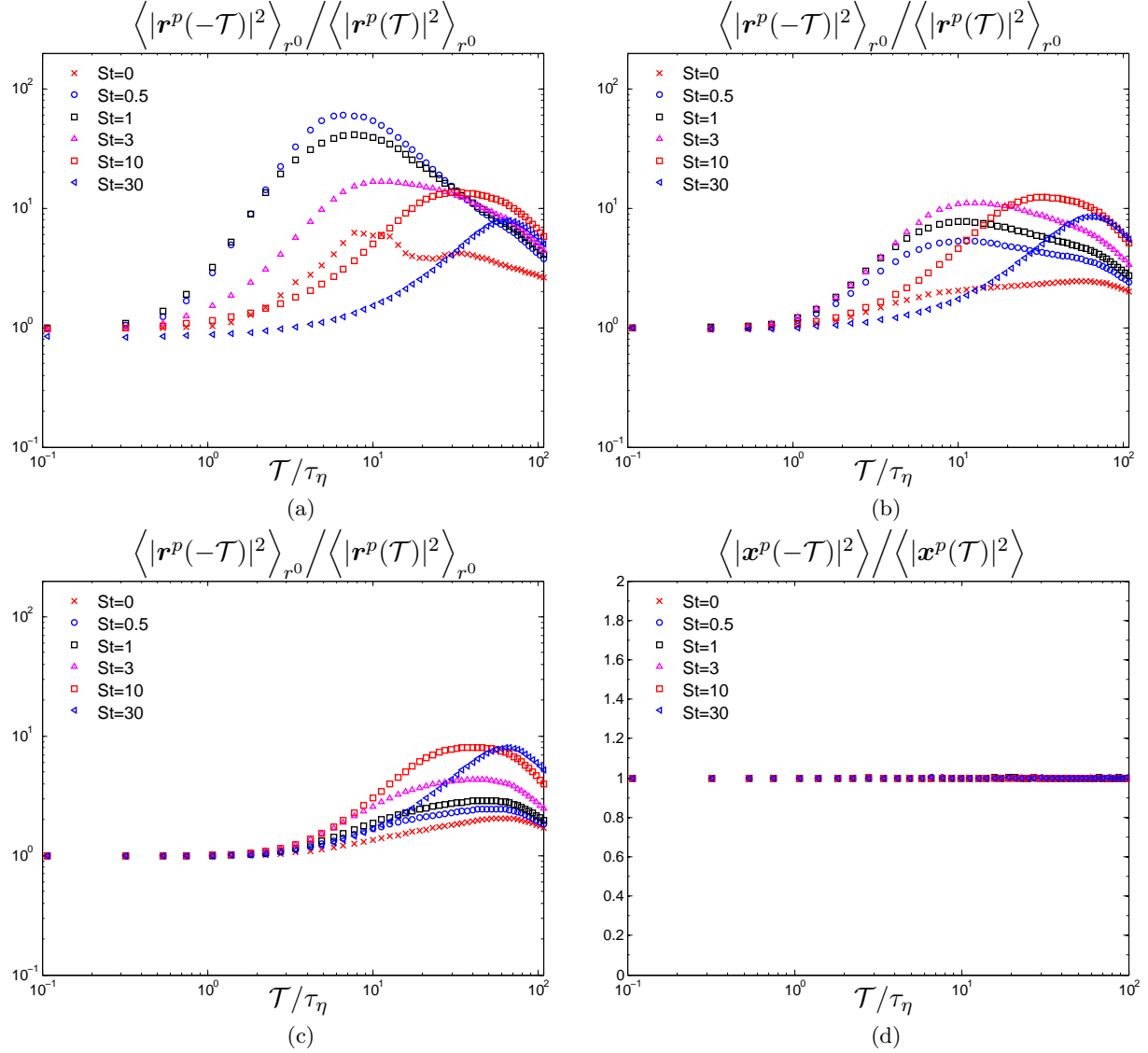


Figure 10: Plots (a)-(c): Ratio of BIT to FIT mean square separation from DNS for (a)  $r^0 \in [0.25\eta, 0.5\eta]$ , (b)  $r^0 \in [3\eta, 4\eta]$ , (c)  $r^0 \in [20\eta, 25\eta]$  and various  $St$ . Plot (d): Ratio of BIT to FIT single particle mean square dispersion from DNS various  $St$ .

In Figure 11 we plot the ratio of the inertial particle to fluid particle BIT mean square separation. Once again the results demonstrate the dramatic effect of inertia on the BIT separation. Notice also, especially in comparing Fig. 10 (a) with Fig. 11 (a), that whereas the time of the peak value of  $\max[\langle |\mathbf{r}^p(-\mathcal{T})|^2 \rangle_{r^0} / \langle |\mathbf{r}^p(\mathcal{T})|^2 \rangle_{r^0}]$  varies significantly with  $St$ , the time of the peak value

of  $\max[\langle |\mathbf{r}^p(-\mathcal{T})|^2 \rangle_{r^0} / \langle |\mathbf{r}^f(-\mathcal{T})|^2 \rangle_{r^0}]$  is approximately independent of  $St$ . In the latter case, this peak time roughly corresponds to  $\tau_{r^0}$  before which the fluid particle separation growth with time is minimal.

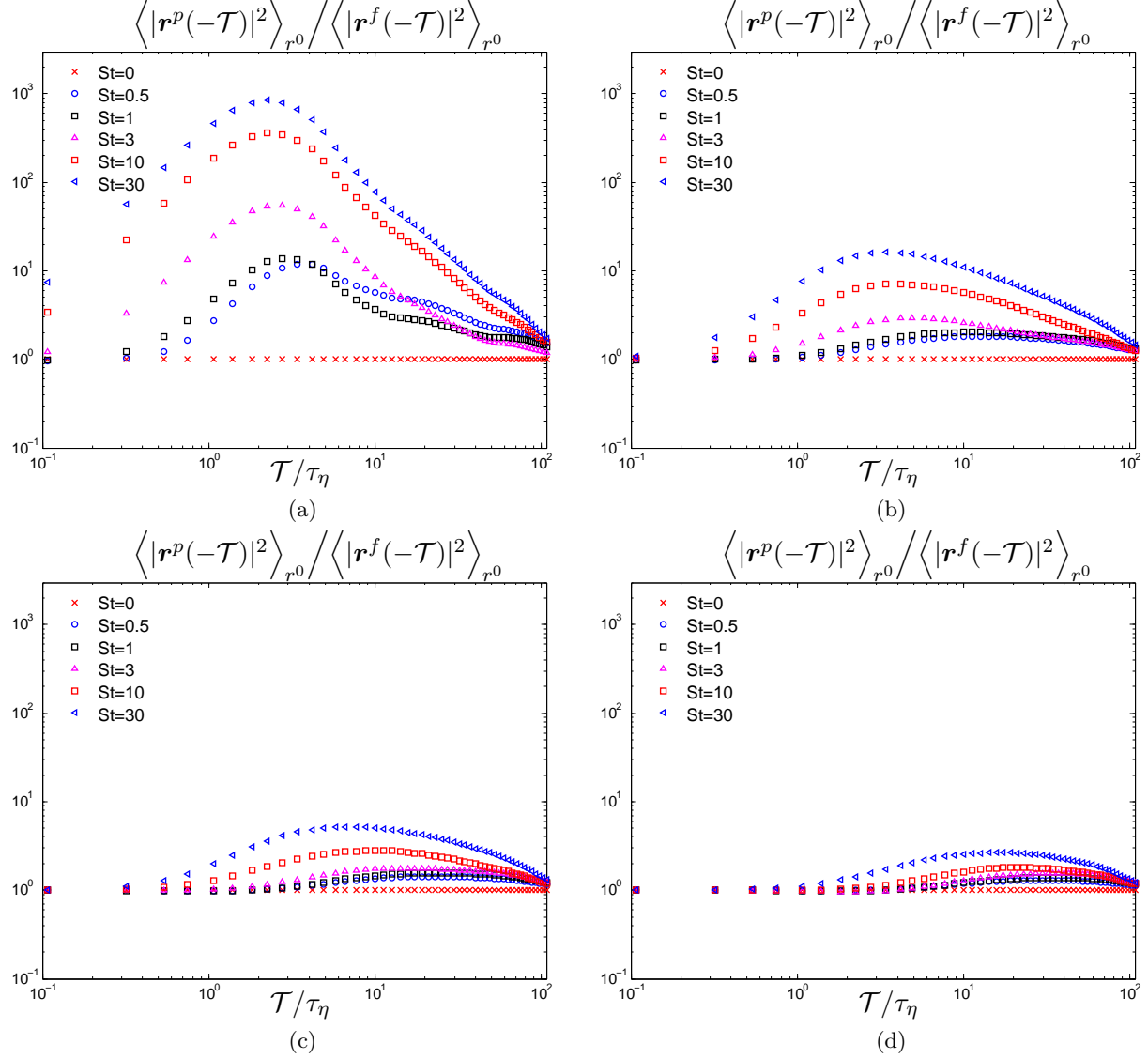


Figure 11: Ratio of inertial particle to fluid particle BIT mean square separation from DNS for (a)  $r^0 \in [0.25\eta, 0.5\eta]$ , (b)  $r^0 \in [3\eta, 4\eta]$ , (c)  $r^0 \in [8\eta, 10\eta]$ , (d)  $r^0 \in [20\eta, 25\eta]$  and various  $St$ .

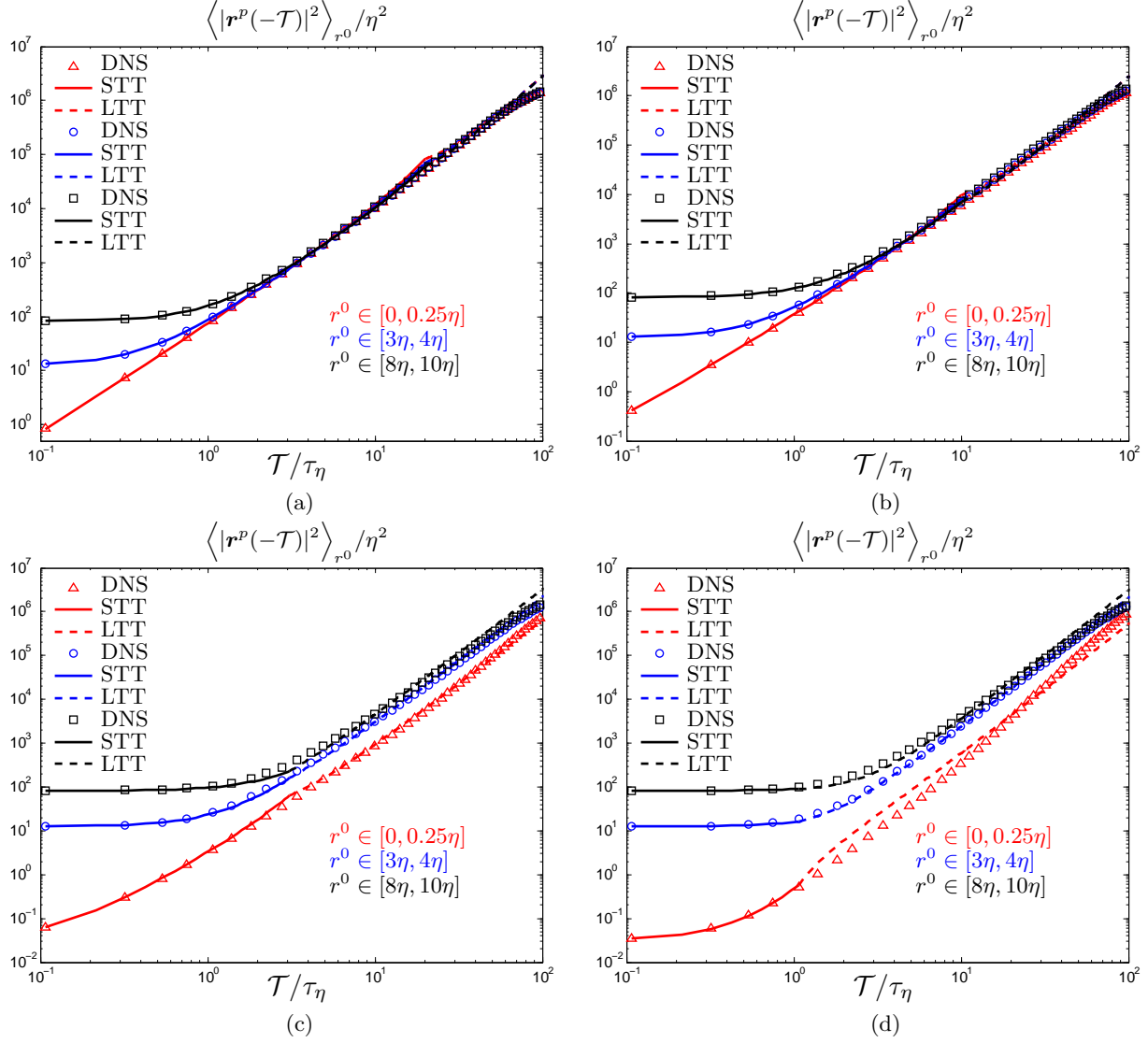


Figure 12: BIT mean square separation for (a)  $St = 20$ , (b)  $St = 10$ , (c)  $St = 3$  and (d)  $St = 1$ . STT - short time theory prediction from Eq.(40). LTT - long time theory prediction from Eq.(46). Colors correspond to different  $r^0$ .

We now compare the DNS results with the theoretical predictions of (40) and (46) in Figure 12. For the long time theory (LTT) predictions given by (46) we suitably tuned the value of  $\mathfrak{g}^B$ , something we will consider in more detail later. The short time theory (STT) contains no adjustable parameters, and the data for  $\langle |\mathbf{w}^p(0)|^2 \rangle_{r^0}$  and  $\langle |\Delta \mathbf{u}^f(0)|^2 \rangle_{r^0}$  required in (40) was taken from the DNS data (shown in Fig. 7).

The results in Fig. 12 show that the STT describes the DNS very accurately for  $\mathcal{T} \leq \hat{\mathcal{T}}$ , capturing the effects of  $St$  and  $r^0$  on the separation in this time regime. The LTT also describes the DNS data well, capturing the separation behavior in the transition from the  $\mathcal{T} \leq \hat{\mathcal{T}}$  behavior up to much larger  $\mathcal{T}$  at which the separation is approximately  $\propto \mathcal{T}^3$ . However, the results show that the LTT does not describe the DNS at very large times ( $\sim 100\tau_\eta$ ). This is simply because at these times the pairs in the DNS have reached integral scale separations at which their separation becomes diffusive, whereas the LTT assumes inertial range scaling for  $\Delta \mathbf{u}^p$  for all  $\mathcal{T} \geq \hat{\mathcal{T}}$  (although it is also possible that at these times the periodicity used in the DNS is affecting their behavior). There is a noticeable discrepancy in Figure. 12 (d) for  $St = 1$ ,  $r^0 \in [0, 0.25\eta]$  for which the LTT does not describe the DNS well. The reason for this is that for  $St = 1$ ,  $r^0 \in [0, 0.25\eta]$ , at  $\mathcal{T} = \hat{\mathcal{T}}$  the root mean square separation is  $< \eta$ . Consequently, the LTT, which uses K41 inertial range scaling to describe  $\Delta \mathbf{u}^p$ , is not applicable. As discussed in §4 for pairs whose separation is still well within the dissipation range at  $\mathcal{T} = \hat{\mathcal{T}}$  we would need to construct a LTT based on a perturbation about the fluid exponential separation law. For the same reasons, at small separations the LTT is not valid for  $St < 1$  also. However we may consider the STT for this regime, as shown in Figure 13.

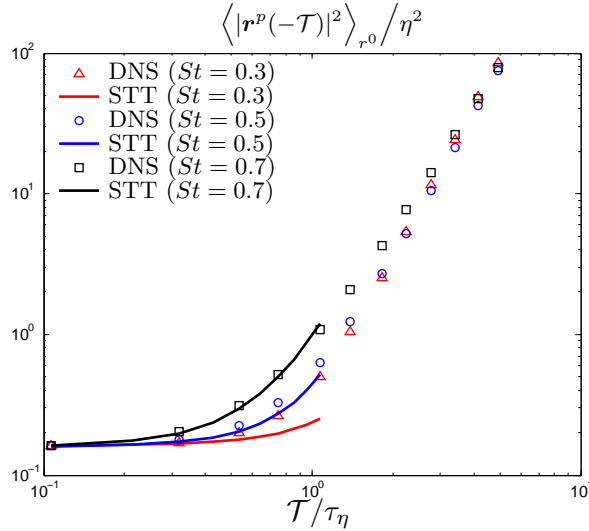


Figure 13: BIT mean square separation for  $r^0 \in [0.25\eta, 0.5\eta]$ . STT - short time theory prediction from Eq.(40).

The results show that although the STT works well for  $St = 0.7$ , it underpredicts the DNS for  $St = 0.3, 0.5$ . A possible explanation for this is that by invoking the approximation in (38) the STT does not fully capture the effect of the preferential sampling of  $\Delta \mathbf{u}$  by the inertial particles (the STT captures some of this effect through  $\langle |\mathbf{w}^p(0)|^2 \rangle_{r^0}$ ). We may consider this effect by not invoking the approximation in (38) so that the STT in (40) would now contain  $\langle |\mathbf{u}^p(0)|^2 \rangle_{r^0}$  instead of  $\langle |\mathbf{u}^f(0)|^2 \rangle_{r^0}$ . In Figure 14 we use the DNS data for  $\langle |\mathbf{u}^p(0)|^2 \rangle_{r^0}$  in this modified STT and compare the predictions with the DNS. Comparing these results with those in Fig. 13 clearly demonstrates that the preferential sampling of the field  $\Delta \mathbf{u}$  by the inertial particles plays an important role on the BIT dispersion at low  $St$ . Furthermore, the results show that with  $\langle |\mathbf{u}^p(0)|^2 \rangle_{r^0}$  correctly specified, the STT is able to accurately describe the BIT dispersion for low  $St$ .



Note that the implication of the results above is that the preferential sampling effect actually increases the rate of dispersion. The reason for this is that in this range the preferential sampling effect gives rise to  $\langle |\mathbf{u}^p(0)|^2 \rangle_{r^0} < \langle |\mathbf{u}^f(0)|^2 \rangle_{r^0}$ . This causes a reduction in the dispersion contribution in the STT coming from the local fluid dynamics such that the dispersion behavior becomes more strongly influenced by the contribution coming from the inertial dynamics of the particles whose dispersion contribution is much faster than the fluid ballistic contribution.

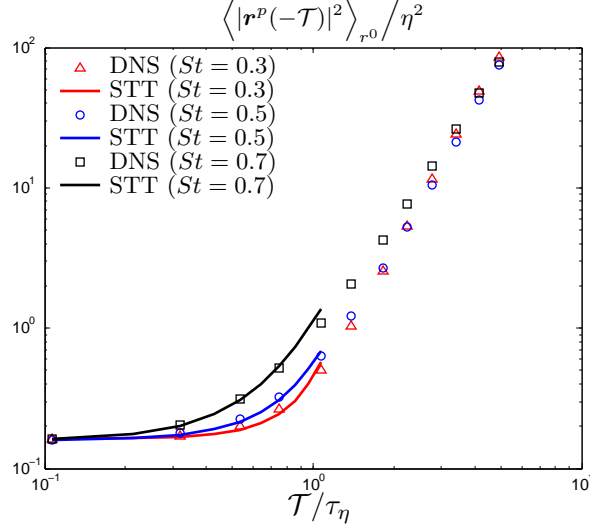


Figure 14: BIT mean square separation for  $r^0 \in [0.25\eta, 0.5\eta]$ . STT - short time theory prediction from Eq.(40) but with  $\langle |\mathbf{u}^f(0)|^2 \rangle_{r^0}$  in the equation replaced with  $\langle |\mathbf{u}^p(0)|^2 \rangle_{r^0}$ , which is here specified by the DNS data.

Finally, recall that in the LTT  $\mathbf{g}^B$  is treated as a tuning parameter since its value for finite  $St$  is not known. We can however in some cases measure it from the DNS data. The results in Figure 15 show that for certain  $St$  and  $r^0$ , the inertial particle long time separation does indeed reach an approximately RO type regime (indicated in the figure by the data tending to a constant), before going to a diffusive type behavior at  $\mathcal{T} \sim 100\tau_\eta$ . Notice that the value at which the curve approximately plateaus (which gives the value  $\mathbf{g}^B(St)$ ) tends to increase with increasing  $St$ . This is again because in BIT dispersion the inertial particles carry a memory of larger scale velocity differences in their path history which enables them to move together faster than fluid particles. In the FIT case, because the particles carry a memory of smaller fluid velocity differences in their path history  $\mathbf{g}^F(St)$  decreases with increasing  $St$ . Recording the value of the curves in Fig. 15 (b) for  $St \leq 3$  at  $\mathcal{T} = 30\tau_\eta$  we obtain an estimate for  $\mathbf{g}^B(St)$ . This data for  $\mathbf{g}^B(St)$  can then be used in the LTT so that the predictions no longer contain any ‘tuning’, and thus constitutes a better test of the LTT. Figure 16 shows the results of using the DNS data to obtain  $\mathbf{g}^B(St)$  for  $St = 1, 3$ . The results in Fig. 16 show that when  $\mathbf{g}^B(St)$  is correctly specified, the LTT accurately describes the dispersion behavior. The discrepancy between the LTT and DNS for  $St = 1$ , and  $r^0 < \eta$  has already been discussed, and the cause explained.

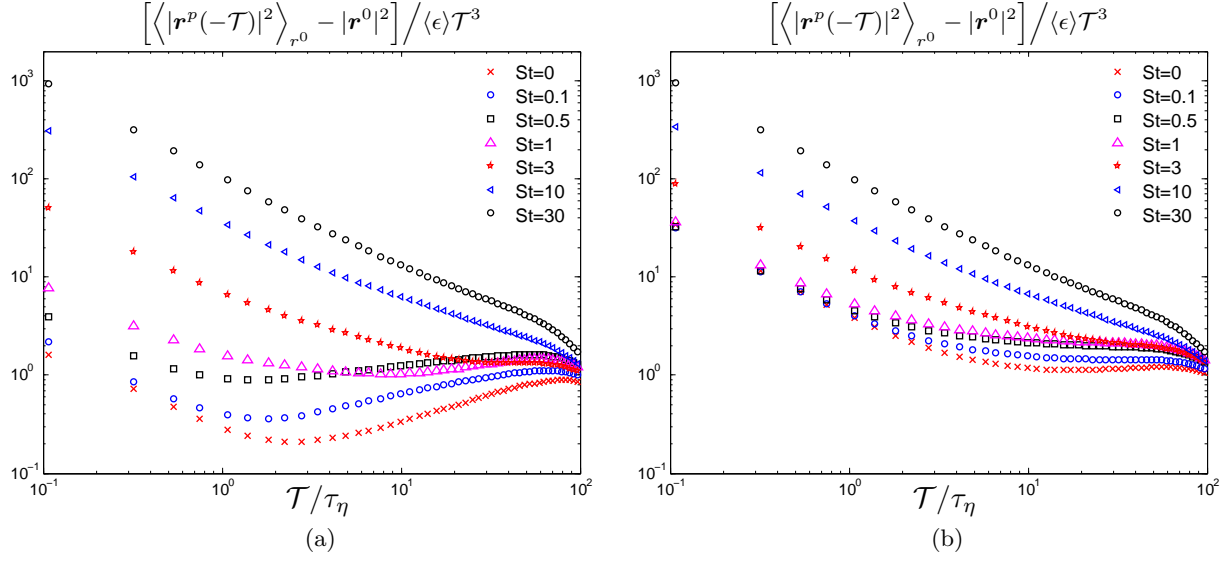


Figure 15: BIT mean square separation divided by  $\langle \epsilon \rangle \mathcal{T}^3$  for (a)  $r^0 \in [0.75\eta, \eta]$ , (b)  $r^0 \in [3\eta, 4\eta]$ .

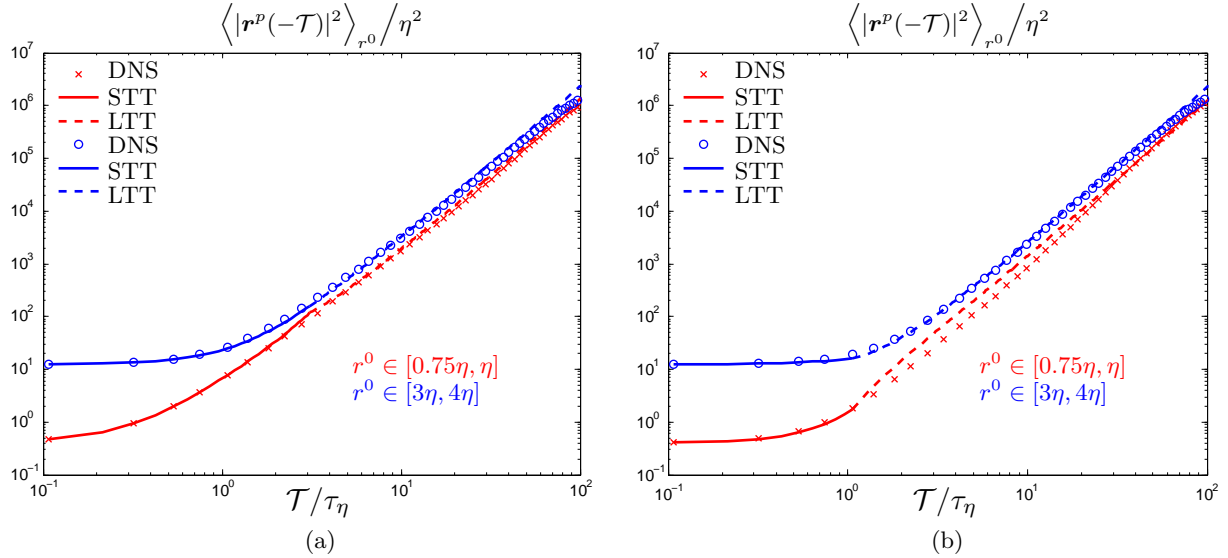


Figure 16: BIT mean square separation for (a)  $St = 3$  and (b)  $St = 1$ . STT - short time theory prediction from Eq.(40). LTT - long time theory prediction from Eq.(46), using DNS data for  $\mathbf{g}^B(St)$ . Colors correspond to different  $r^0$ .

## 5 Conclusion

In this paper we have considered the FIT and BIT dispersion of fluid and inertial particles. The FIT and BIT dispersion of inertial particles are qualitatively and quantitatively different with BIT dispersion occurring at a much greater rate. In general the time irreversibility of inertial particle relative dispersion is much greater than that for fluid particles. This is because inertial particle pair relative dispersion is subject to both the time irreversibility of the underlying turbulence and also that due to the history effect of their inertia.

Concerning the FIT and BIT dispersion of fluid particles, our DNS data shows that the dispersion is accurately described for short times by the ballistic law for all separations. A new result was derived for fluid particle dispersion in the dissipation regime which captures the transition from the initial ballistic to the later exponential separation, and is in excellent agreement with the DNS data. We also observe clear RO scaling for initial separations lying between 3 and 4  $\eta$ , and the FIT and BIT Richardson's constants were found to be in excellent agreement with experimental data. For smaller separations the contaminating effect of the small scale separation behavior means that the RO law is never attained for the time spans we have data, although it does appear to be approaching this asymptotically. For larger initial separations the limited scale separation in our DNS means that the RO law is not reached by the time the fluid particle pairs are at integral scale separations.

We also developed theoretical predictions for the BIT dispersion of inertial particles. The small time theory which describes the separation of the particles for times  $\leq \max[\tau_p, \tau_{r0}]$  agrees very well with DNS data. For times  $> \max[\tau_p, \tau_{r0}]$  we developed a result which is essentially a perturbation about the RO law. The predictions from this long time theory were found to be in good agreement with the DNS provided that their separations at these times exceeds a few multiples of  $\eta$ . However, this large time theory contains an adjustable parameter, the backward in time Richardson constant for inertial particles which requires tuning. Nevertheless, in some cases this can be obtained from the DNS, and when this value is used in the large time theory, the predictions are again in very good agreement with the DNS.

The research presented in this paper will be of use for understanding mixing processes of inertial particles in turbulence, which is connected to BIT and not FIT dispersion. We have shown how dramatically the BIT and FIT dispersion can differ for inertial particles, highlighting how inappropriate it may be to approximate them as being equivalent in mixing models for inertial particles. The work is also important for the development of the theory presented in [9] for the relative velocities of inertial particles in isotropic turbulence. In [9] they approximated the BIT mean square separation by its FIT counterpart since no theory or data was available to inform them of the BIT behavior. In [10] we argued that this approximation is responsible for some error in their theory predictions. In future work we intend to develop the theory presented in [9] by using the BIT closures developed in this paper.

## A Description of DNS

In this appendix we describe the DNS used in the paper. For a detailed description see [25]; here we give a brief summary.

We use a pseudospectral method to solve the incompressible Navier-Stokes equations for statistically stationary isotropic turbulence in a three-dimensional periodic cube of length  $2\pi$ ,

$$\frac{\partial \mathbf{u}}{\partial t} + \boldsymbol{\omega} \times \mathbf{u} + \frac{\partial}{\partial \mathbf{x}} \left( \frac{p}{\rho} + \frac{\mathbf{u} \cdot \mathbf{u}}{2} \right) = \nu \frac{\partial}{\partial \mathbf{x}} \cdot \frac{\partial \mathbf{u}}{\partial \mathbf{x}} + \mathbf{f}, \quad (49)$$

where  $\mathbf{u}$  is the fluid velocity,  $\boldsymbol{\omega}$  is the vorticity,  $p$  is the pressure,  $\rho$  is the fluid density,  $\nu$  is the kinematic viscosity, and  $\mathbf{f}$  is a large-scale forcing function that is added to achieve stationary turbulence. For this simulation, forcing was added to the first two wavenumbers in Fourier space. Time integration is performed through a second-order, explicit Runge-Kutta scheme with aliasing errors removed by means of a combination of spherical truncation and phase-shifting. The time step was chosen to achieve a CFL number of about 0.5.

The fluid field was solved on a grid with  $2048^3$  grid points on 16,384 processors on the Yellowstone cluster at the U.S. National Center for Atmospheric Research. The three-dimensional fast Fourier transforms required for the pseudospectral solution of (49) are performed in parallel with MPI using the P3DFFT library [26]. The Taylor microscale Reynolds number  $R_\lambda$  for our flow is about 580 and the ratio  $L/\eta \approx 800$ , making this the highest Reynolds number and largest scale separation studied to date for inertial-particle-laden isotropic turbulence.

The flow was initialized by mapping an existing isotropic flow field with  $512^3$  grid points onto the  $2048^3$  grid. The viscosity was chosen to achieve a small-resolution  $k_{\max}\eta \approx 1.7$  (where  $k_{\max} = 2048\sqrt{2}/3$  is the maximum resolved wavenumber magnitude). This initial flow field was then evolved for about 5 large eddy turnover times until the flow statistics were statistically stationary.

For comparison with the theory the particle equation of motion is the simplified form of the Maxey-Riley equation [11]

$$\frac{d^2}{dt^2}\mathbf{x}^p = \frac{d}{dt}\mathbf{v}^p = \frac{1}{\tau_p}\left(\mathbf{u}(\mathbf{x}^p(t), t) - \mathbf{v}^p(t)\right), \quad (50)$$

where  $\mathbf{x}^p(t)$  and  $\mathbf{v}^p(t)$  are the particle position and velocity vectors and  $\mathbf{u}(\mathbf{x}^p(t), t)$  is the fluid velocity at the particle position which is calculated using an eight-point B-spline interpolation [27]. Fluid particles were also tracked by solving  $\dot{\mathbf{x}}^f(t) = \mathbf{u}(\mathbf{x}^f(t), t)$ .

A total of 18 different particle classes were simulated, with Stokes numbers, defined as  $St = \tau_p/\tau_\eta$ , ranging from 0 to 30. About 17 million particles were tracked for each value of  $St$  for a total of 300 million particles. At the initial time, particles were injected in the flow with a uniform distribution. The particles were allowed to equilibrate with the statistically stationary flow field for about 5 large-eddy turnover times before we began gathering statistics. Measurement of the particle radial distributions and velocities confirmed that the particle field had reached a statistically stationary state after this development time.

The mean square separation calculations are carried out over a total time of  $100\tau_\eta$ , or about 1.6 large eddy turnover times, and particle positions and velocities were stored approximately every  $0.1\tau_\eta$ .

## References

- [1] G. I. Taylor. Diffusion by continuous movements. *Proc. Lond. Math. Soc.*, 20:196–212, 1922.
- [2] L. F. Richardson. Atmospheric diffusion shown on a distance-neighbour graph. *Proc. R. Soc. London Ser. A*, 110:709–737, 1926.
- [3] B. L. Sawford. Turbulent relative dispersion. *Annu. Rev. Fluid Mech.*, 33:289–317, 2001.
- [4] J. P. L. C. Salazar and L. R. Collins. Two-particle dispersion in isotropic turbulent flows. *Annu. Rev. Fluid Mech.*, 41:405–432, 2009.
- [5] B. L. Sawford, P.-K. Yeung, and M. S. Borgas. Comparison of backwards and forwards relative dispersion in turbulence. *Phys. Fluids*, 17:095109, 2005.

- [6] J. Bec, L. Biferale, A. S. Lanotte, A. Scagliarini, and F. Toschi. Turbulent pair dispersion of inertial particles. *J. Fluid Mech.*, 645:497–528, 2010.
- [7] I. Fouxon and P. Horvai. Separation of heavy particles in turbulence. *Phys. Rev. Lett.*, 100:040601, 2008.
- [8] J. Bec, M. Cencini, R. Hillerbrand, and K. Turitsyn. Stochastic suspensions of heavy particles. *Physica D*, 237:2037–2050, 2008.
- [9] L. Pan and P. Padoan. Relative velocity of inertial particles in turbulent flows. *J. Fluid Mech.*, 661:73–107, 2010.
- [10] A.D. Bragg and L.R. Collins. New insights from comparing statistical theories for inertial particles in turbulence. part ii. relative velocities of particles. *New J. Phys. (under review)*, 2013.
- [11] M. R. Maxey and J. J. Riley. Equation of motion for a small rigid sphere in a nonuniform flow. *Phys. Fluids*, 26:883–889, 1983.
- [12] G. K. Batchelor. The application of the similarity theory of turbulence to atmospheric diffusion. *Quart. J. Roy. Meteorol. Soc.*, 76:133–146, 1950.
- [13] N. T. Ouellette, H. Xu, M. Bourgoin, and E. Bodenschatz. An experimental study of turbulent relative dispersion models. *New J. Phys.*, 8:109, 2006.
- [14] J. P. L. C. Salazar and L. R. Collins. Inertial particle relative velocity statistics in homogeneous isotropic turbulence. *J. Fluid Mech.*, 696:45–66, 2012.
- [15] G. K. Batchelor. The effect of homogeneous turbulence on material lines and surfaces. *Proc. R. Soc. Lond. A*, 213:349–366, 1952.
- [16] Takashi Ishihara, Toshiyuki Gotoh, and Yukio Kaneda. Study of high-Reynolds-number isotropic turbulence by direct numerical simulation. *Annu. Rev. Fluid Mech.*, 41:165–180, 2009.
- [17] Jacob Berg, B. Lüthi, J. Mann, and S. Ott. Backwards and forwards relative dispersion in turbulent flow: An experimental investigation. *Phys. Rev. E*, 74:016304, 2006.
- [18] T. Faber and J. C. Vassilicos. Turbulent pair separation due to multi-scale stagnation point structure and its time asymmetry in two-dimensional turbulence. *Phys. Fluids*, 21:015106, 2009.
- [19] B. L. Sawford, P.-K. Yeung, and J. F. Hackl. Reynolds number dependence of relative dispersion statistics in isotropic turbulence. *Phys. Fluids*, 20:065111, 2008.
- [20] R. Bitane, H. Homann, and J. Bec. Time scales of turbulent relative dispersion. *Phys. Rev. E*, 86:045302, 2012.
- [21] J. Bec, L. Biferale, M. Cencini, A. S. Lanotte, and F. Toschi. Intermittency in the velocity distribution of heavy particles in turbulence. *J. Fluid Mech.*, 646:527–536, 2010.
- [22] E. A. Novikov. The effects of intermittency on statistical characteristics of turbulence and scale similarity of breakdown coefficients. *Phys. Fluids. A*, 2:814–820, 1990.

- [23] G. Boffetta, A. Celani, A. Crisanti, and A. Vulpiani. Relative dispersion in fully developed turbulence: Lagrangian statistics in synthetic flows. *Europhys. Lett.*, 46:177–182, 1999.
- [24] F. G. Schmitt. Explicit predictability and dispersion scaling exponents in fully developed turbulence. *Phys. Lett. A.*, 342:448–458, 2005.
- [25] P. J. Ireland, T. Vaithianathan, P. S. Sukheswalla, B. Ray, and L. R. Collins. Highly parallel particle-laden flow solver for turbulence research. *Comput. Fluids*, 76:170–177, 2013.
- [26] D. Pekurovsky. P3DFFT: A framework for parallel computations of Fourier transforms in three dimensions. *SIAM J. Sci. Comput.*, 34(4):C192–C209, 2012.
- [27] M. A. T. van Hinsberg, J. H. M. Thije Boonkamp, F. Toschi, and H. J. H. Clercx. On the efficiency and accuracy of interpolation methods for spectral codes. *SIAM J. Sci. Comput.*, 34(4):B479–B498, 2012.